Neuron
Article

Distinct Modes of AMPA Receptor Suppression at Developing Synapses by GluN2A and GluN2B: Single-Cell NMDA Receptor Subunit Deletion In Vivo

John A. Gray,[1] Yun Shi,[1] Hiroshi Usui,[3] Matthew J. During,[4] Kenji Sakimura,[3] and Roger A. Nicoll[1,2,*]
[1]Department of Cellular and Molecular Pharmacology
[2]Department of Physiology
University of California, San Francisco, CA, 94143, USA
[3]Department of Cellular Neurobiology, Brain Research Institute, Niigata University, Niigata 951-8585, Japan
[4]Departments of Molecular Virology, Immunology, and Medical Genetics, Ohio State University, Columbus, OH, 43210, USA
*Correspondence: roger.nicoll@ucsf.edu
DOI 10.1016/j.neuron.2011.08.007

SUMMARY

During development there is an activity-dependent switch in synaptic *N*-Methyl-D-aspartate (NMDA) receptor subunit composition from predominantly GluN2B to GluN2A, though the precise role of this switch remains unknown. By deleting GluN2 subunits in single neurons during synaptogenesis, we find that both GluN2B and GluN2A suppress AMPA receptor expression, albeit by distinct means. Similar to GluN1, GluN2B deletion increases the number of functional synapses, while GluN2A deletion increases the strength of unitary connections without affecting the number of functional synapses. We propose a model of excitatory synapse maturation in which baseline activation of GluN2B-containing receptors prevents premature synapse maturation until correlated activity allows induction of functional synapses. This activity also triggers the switch to GluN2A, which dampens further potentiation. Furthermore, we analyze the subunit composition of synaptic NMDA receptors in CA1 pyramidal cells, provide electrophysiological evidence for a large population of synaptic triheteromeric receptors, and estimate the subunit-dependent open probability.

INTRODUCTION

The formation and maturation of developing excitatory synapses involves precise regulation of the expression and incorporation of ionotropic glutamate receptors responsible for accurate information transfer between neurons. A central feature characterizing the maturation of glutamatergic synapses is a shift from predominantly *N*-Methyl-D-aspartate (NMDA) receptor-mediated to alpha-amino-3-hydroxy-5-methyl-4- isoxazolepropionic acid (AMPA) receptor-mediated neurotransmission during the first few postnatal weeks in rodents (Crair and Malenka, 1995; Hsia et al., 1998). Experience-driven activity through NMDA receptors promotes the maturation of excitatory circuitry during brain development (Durand et al., 1996; Liao et al., 1999). NMDA receptors (NMDARs) play well-known roles in the bidirectional regulation of synaptic AMPA receptor (AMPAR) content at mature hippocampal synapses through the processes of long-term potentiation (LTP) and long-term depression (LTD) (Malenka and Bear, 2004). However, the molecular mechanisms that regulate synaptic AMPAR content at developing synapses are likely distinct from those mediating LTP and LTD at mature synapses (Groc et al., 2006; Hall and Ghosh, 2008; Yasuda et al., 2003). Indeed, accumulating evidence suggests that AMPARs can be recruited to nascent synapses in the absence of NMDAR signaling (Adesnik et al., 2008; Colonnese et al., 2003; Friedman et al., 2000; Tsien et al., 1996; Ultanir et al., 2007). Thus, while the incorporation of AMPARs into mature synapses is widely associated with the activation of NMDARs, NMDAR signaling at nascent synapses actually restricts AMPAR currents.

Functional NMDARs are heteromeric assemblies containing two obligatory GluN1 subunits and two regulatory subunits, usually GluN2 subunits of which there are four isoforms (GluN2A, GluN2B, GluN2C, and GluN2D). These GluN2 subunits confer distinct functional properties to the NMDARs by influencing current kinetics and the complement of associated intracellular signaling proteins (Cull-Candy and Leszkiewicz, 2004; Monyer et al., 1994; Vicini et al., 1998). In addition, at most forebrain excitatory synapses, the NMDAR subunit composition changes during development with predominantly GluN2B-containing NMDARs early in development gradually replaced or supplemented by "mature" GluN2A-containing NMDARs (Flint et al., 1997; Roberts and Ramoa, 1999; Sheng et al., 1994). This shift in the ratio of GluN2A/GluN2B is thought to alter the threshold for inducing NMDAR-mediated synaptic plasticity (Yashiro and Philpot, 2008). Moreover, the switch from GluN2B- to GluN2A-containing NMDARs is bidirectionally regulated by experience and activity (Bellone and Nicoll, 2007; Quinlan et al., 1999). Given the developmental and activity-dependent regulation of the relative expression and distribution of GluN2 subunits, an increased understanding of the developmental impact of this subunit switch will yield insight into multiple aspects of synaptic function.

Many studies have aimed at ascertaining the precise role of NMDARs and GluN2 subunits in the development of cortical circuitry; however, most have relied on widespread pharmacological inhibition or broad genetic deletions (Colonnese et al., 2003; Hahm et al., 1991; Iwasato et al., 2000). These approaches are problematic for a number of reasons. First, while GluN2A knockout (KO) mice are fully viable (Sakimura et al., 1995), GluN2B KO mice die perinatally (Kutsuwada et al., 1996), similar to GluN1 KO mice (Forrest et al., 1994; Li et al., 1994). Furthermore, germline deletion of an NMDAR allele has the potential to disrupt developing circuits, leading to altered or compensatory pathways that result in a false readout of the cell autonomous effects of subunit deletion. Moreover, pharmacologic inhibition and traditional KOs cannot separate the cell-autonomous role of NMDARs and GluN2 subunits from indirect effects on network activity associated with a broad loss of NMDAR function (Turrigiano et al., 1998). Indeed, NMDAR antagonists potently alter afferent patterning in visual areas (Colonnese et al., 2005) and can promote remodeling of thalamic neurons (Hahm et al., 1991). Furthermore, pharmacologic blockade has been reported to massively reorganize and cluster NMDARs in neurons, which could have various downstream effects (Rao and Craig, 1997), and interpretation of GluN2 subunit-specific inhibition is problematic (Neyton and Paoletti, 2006). Due to the lethality of germline GluN2B deletion, RNA interference in cultured neurons has been used recently to examine the effects of GluN2B at single cells (Foster et al., 2010; Hall et al., 2007). However, these results are accompanied by a large reduction in GluN2A expression.

To minimize potential indirect effects on developing network activity, we abolished NMDAR subunits in sparsely distributed cells in the hippocampus by introducing Cre recombinase into neurons in conditional KO mice for GluN2A and GluN2B. This mosaic deletion allows for simultaneous paired whole-cell recordings from Cre-expressing and untransfected neighboring cells, providing a rigorous, quantitative, and internally controlled comparison of the cell-autonomous effects of GluN2 subunit deletion. By deleting GluN2A or GluN2B during early postnatal development, a period of rapid synaptogenesis, we found that both subunits negatively regulate synaptic AMPAR expression, but by distinct means. We show that, similar to GluN1 deletion (Adesnik et al., 2008), deletion of GluN2B increases the number of functional synapses, suggesting a basal role for GluN2B-containing NMDARs in maintaining silent synapses in early development. Conversely, deletion of GluN2A increases synaptic strength without affecting the number of unitary connections. These results suggest that when significant bursts of activity drive the synaptic insertion of AMPARs and the recruitment of GluN2A-containing receptors, GluN2A functions to dampen further synapse potentiation.

RESULTS

GluN2A and GluN2B are the Only GluN2 Subunits Contributing to Synaptic NMDAR-EPSCs in CA1 Pyramidal Neurons

The hippocampal CA3-to-CA1 synapse is a model excitatory synapse that has been used to delineate the mechanisms of synaptic plasticity. Using conditional KO alleles for GluN2A (*Grin2a*$^{fl/fl}$; see Figure S1A available online) and GluN2B (*Grin2b*$^{fl/fl}$) (Akashi et al., 2009), we eliminated the target gene in a small subset of hippocampal neurons by transcranial stereotactic injection of P0-P1 mice with a recombinant adeno-associated virus expressing a Cre-GFP fusion protein (rAAV1-Cre-GFP) (Kaspar et al., 2002). Figure 1A shows a typical acute slice made from a P18 mouse after P0 injection demonstrating sparse infection of CA1 pyramidal neurons.

It has long been suspected from in situ hybridization, single-cell reverse-transcriptase polymerase chain reaction, and pharmacologic studies that hippocampal CA1 pyramidal neurons express primarily GluN2A and GluN2B subunits (Garaschuk et al., 1996; Watanabe et al., 1992; Zhong et al., 1995). By crossbreeding the *Grin2a*$^{fl/fl}$ (ΔGluN2A) and *Grin2b*$^{fl/fl}$ (ΔGluN2B) mice, we generated *Grin2a*$^{fl/fl}$*Grin2b*$^{fl/fl}$ (ΔGluN2AΔGluN2B) mice and simultaneous whole-cell recording from a Cre-expressing cell (green trace in inset), and a control cell in the presence of NBQX revealed a complete loss of NMDAR-EPSCs (Figure 1B, inset). We followed the time course of subunit depletion by measuring the ratio of NMDAR-EPSCs from Cre-expressing cells to control cells after P0 injection, and demonstrated a gradual decrease in NMDAR-EPSCs and complete loss consistently by P15 (Figure 1B), similar to the rate of loss of NMDAR-EPSCs in *Grin1*$^{fl/fl}$ mice (ΔGluN1). These data indicate that, in addition to obligatory GluN1 subunits, synaptic NMDA receptors in CA1 pyramidal neurons contain only GluN2A and GluN2B.

Since the NMDA-EPSCs were entirely gone by P15 in the double conditional KO mice, we performed all subsequent analyses of ΔGluN2A and ΔGluN2B mice after P17 unless indicated. In Figure 1C, NMDAR-EPSCs were obtained, averaged, and peak-aligned from Cre-expressing or control cells in ΔGluN2A and ΔGluN2B mice in the presence of NBQX. As expected, the average NMDAR-EPSC decay times (τ_w) recorded from Cre-expressing cells from ΔGluN2A mice were significantly slower than cells from ΔGluN2B mice and control cells. Importantly, decay rate was not affected by the amplitude of the NMDAR-EPSC, indicating effective space clamp (Figure S1B). Normalizing and aligning the traces at the stimulus onset (Figure 1D) shows that NMDAR-EPSCs from ΔGluN2B cells have a significantly faster rise than ΔGluN2A cells, with control cells intermediate. These results are consistent with rise times and decays previously described for diheteromeric GluN1/GluN2A and GluN1/GluN2B receptors in heterologous systems (Vicini et al., 1998) and suggest that the Cre-expressing cells have pure diheteromeric populations of synaptic NMDARs. Since GluN2C and GluN2D subunits have lower sensitivity to Mg^{2+} blockade compared with GluN2A and GluN2B subunits (Monyer et al., 1992), we examined the voltage-dependent Mg^{2+} sensitivity of the NMDAR-EPSCs in Cre-expressing ΔGluN2A and ΔGluN2B cells. As shown in Figure 1E, there is a high level of voltage-dependent Mg^{2+} block in Cre-expressing ΔGluN2A and ΔGluN2B cells that was indistinguishable from control cells, further excluding a measurable contribution of diheteromeric GluN2C- or GluN2D-containing NMDARs.

Previous studies have shown that the decay rate of NMDAR-EPSCs is voltage-dependent in the absence of Mg^{2+} (Hestrin, 1992; Konnerth et al., 1990) and that early in development (<5 weeks) the decay is slower at positive potentials while in

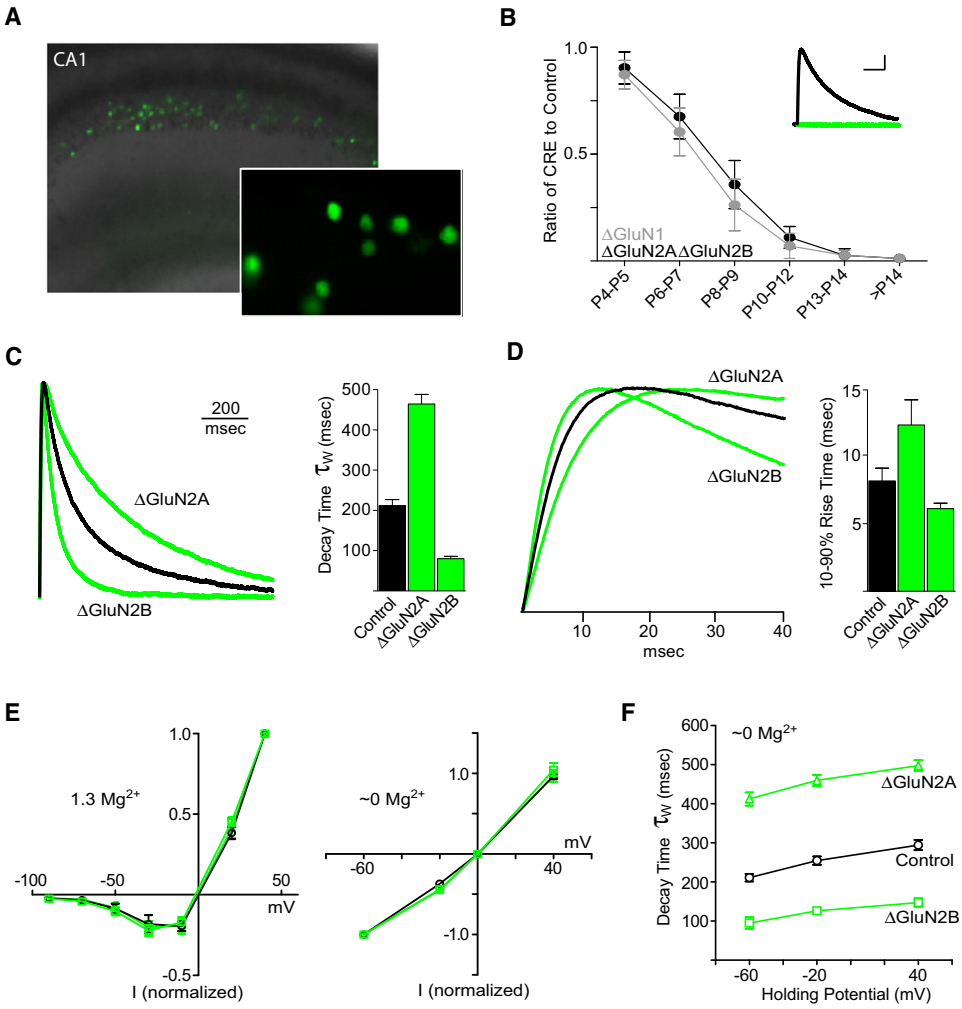

Figure 1. Characterization of Single-Cell GluN2A, GluN2B, or Double Deletion

(A) Epifluorescence images (left, low magnification; inset, high magnification) show mosaic expression of Cre-GFP in the CA1 region of a typical acute hippocampal slice made from a P18 mouse injected at P0 with rAAV1-Cre-GFP. Cre expression, and thus GFP, is confined to the nucleus.

(B) Time course of changes in evoked NMDAR-EPSC amplitude in *Grin1*$^{fl/fl}$ (gray) and *Grin2a*$^{fl/fl}$*Grin2b*$^{fl/fl}$ (black) mice after P0 injection of rAAV1-Cre-GFP expressed as the mean ± SEM of the ratios of simultaneously recorded NMDAR-EPSCs from Cre to control cells recorded at +40 mV in the presence of 10 μM NBQX (n = 3–6 for each group from P4-P14, n = 10–21 for >P14); inset, representative traces from a P18 paired recording from *Grin2a*$^{fl/fl}$*Grin2b*$^{fl/fl}$ mice (control, black; transfected, green; scale bar represents 20 pA, 200 ms).

(C) Averaged and peak-aligned NMDAR-EPSCs from transfected or control cells from *Grin2a*$^{fl/fl}$ or *Grin2b*$^{fl/fl}$ mice at P18-P22 after P0 injection recorded at +40 mV in the presence of 10 μM NBQX. Bar graph shows the NMDAR-EPSC decay expressed as a weighted Tau (control, 212.0 ± 14.9 msec, n = 35; ΔGluN2A, 467.1 ± 24.1 msec, n = 29; ΔGluN2B, 80.1 ± 5.9 msec, n = 26).

(D) Averaged and base-aligned NMDAR-EPSCs. Bar graph shows the NMDAR-EPSC 10%–90% rise time (control, 8.2 ± 0.9 msec, n = 35; ΔGluN2A, 12.4 ± 1.9 msec, n = 29; ΔGluN2B, 6.1 ± 0.4 msec, n = 26).

(E) I/V curves of NMDAR-EPSCs recorded at various holding potentials with 1.3 mM (left) or 0 mM (right) Mg^{2+}. Junction potentials were corrected (control, black; ΔGluN2A and ΔGluN2B, green).

(F) NMDAR-EPSC decay times expressed as a weighted Tau from transfected or control cells from P20-P25 animals recorded at various holding potentials in the presence of 10 μM NBQX in 0 mM Mg^{2+}. See also Figure S1.

All data represent mean ± SEM.

older mice the decay is faster at positive potentials (Kirson and Yaari, 1996). This developmental switch in the direction of voltage-dependent decay rate may be related to GluN2 subunit composition. However, as shown in Figure 1F, NMDAR-EPSC decay kinetics are slower at positive holding potentials regardless of subunit composition.

NMDAR Open Probability is Differentially Modulated by GluN2 Subunits

Studies in heterologous systems have suggested that the probability of NMDAR opening in response to glutamate is dependent on the GluN2 subunit composition, with GluN2A imparting a higher open probability (P_O) than GluN2B (Chen et al., 1999;

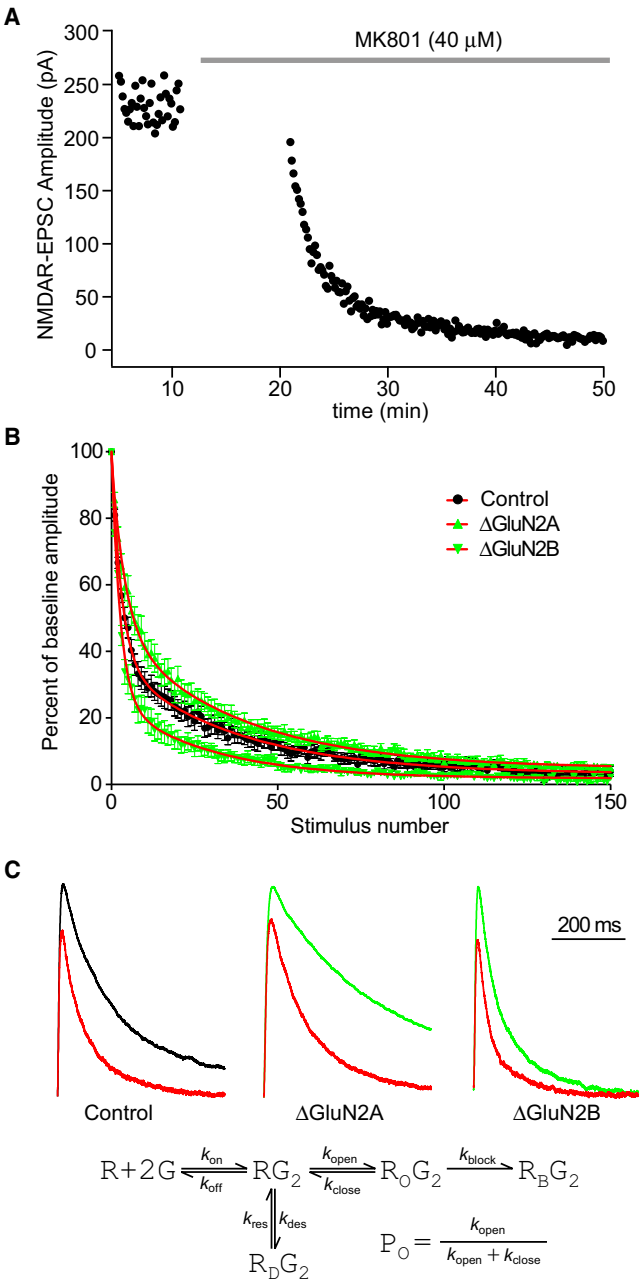

Figure 2. Open Probability of Synaptic NMDARs Depends on GluN2 Subunit Composition

(A-C) Decrease of evoked NMDAR-EPSC amplitudes in MK801 from transfected or control cells from *Grin2a*$^{fl/fl}$ or *Grin2b*$^{fl/fl}$ mice at P17-P21 after P0 injection.

(A) Representative experiment plotting NMDAR-EPSC amplitude against time. A stable baseline was obtained, stimulation was stopped for 10 min as 40 μM MK801 was perfused onto the slice, and then stimulation was restarted.

(B) NMDAR-EPSC amplitudes were normalized to the average baseline amplitude and plotted as a function of stimulus number, and each group was fit with a double exponential decay (control, n = 10; ΔGluN2A, n = 7; ΔGluN2B, n = 11; error bars represent SEM).

(C) Normalized and averaged traces of the baseline NMDAR-EPSC and the first pulse in the presence of MK801 (red). Each experiment was fitted by a five-state kinetic model (bottom) (Clements and Westbrook, 1991). Open probability (P_O) was estimated to be 0.26 for control cells, 0.21 for ΔGluN2A, and 0.39 for ΔGluN2B. See also Figure S2.

Erreger et al., 2005). However, the differential effect of GluN2 subunits on NMDAR open probability has been challenged by previous work in neurons (Chavis and Westbrook, 2001; Prybylowski et al., 2002). Using the pure diheteromeric GluN1/GluN2A and GluN1/GluN2B synaptic populations, we assessed NMDAR open probability using MK801, an open channel blocker that is effectively irreversible and has been used to estimate P_O (Huettner and Bean, 1988; Jahr, 1992). For each recording, a stable NMDAR-EPSC was obtained, stimulation was stopped for 10 min as 40 μM MK801 was perfused onto the slice, and then stimulation was restarted (Figure 2A). A greater rate of MK801 block was seen with ΔGluN2B than with ΔGluN2A (Figure 2B), suggesting a higher P_O in the absence of differences in the presynaptic release probability (see Figure 5D). To obtain an estimate of P_O, the baseline NMDAR-EPSC and the first EPSC after perfusion of MK801 were fitted to a simplified 5-state NMDAR gating model (Figure 2C; Figure S2) (Clements and Westbrook, 1991). The P_O of GluN1/GluN2A (0.39) was significantly higher than GluN1/GluN2B (0.21), while NMDARs from control cells had an intermediate P_O (0.26).

CA1 Pyramidal Neurons Undergo Incomplete NMDAR Subunit Switching and Contain Significant Levels of Triheteromeric Receptors

Ifenprodil and its derivatives are the only sufficiently subtype-selective NMDAR antagonists (Neyton and Paoletti, 2006). Ifenprodil is a negative allosteric modulator of GluN1/GluN2B receptors with >200-fold selectivity over other GluN2 subunits (Williams, 1993) and has frequently been used to differentiate the roles of GluN2 subtypes in multiple synaptic and cellular processes. Ifenprodil binds to the N-terminal domain of GluN2B in a use-dependent and voltage-independent manner (Perin-Dureau et al., 2002; Williams, 1993) and produces approximately 80% inhibition of GluN1/GluN2B receptors in heterologous systems (Tovar and Westbrook, 1999). Thus, we wanted to examine the effects of ifenprodil on pure synaptic populations of GluN1/GluN2A and GluN1/GluN2B. In Figure 3A, we show that 3 μM ifenprodil maximally inhibits NMDAR-EPSCs as predicted for pure diheteromeric GluN1/GluN2B but has no significant effect on a pure population of GluN1/GluN2A and an intermediate effect on wild-type (WT) receptors. Notably, many studies have used 10 μM ifenprodil for selective inhibition of GluN2B, but we found that 10 μM ifenprodil produces approximately 15% inhibition of GluN1/GluN2A receptors (Figure S3A) with no increase in the block of GluN1/GluN2B receptors. Interestingly, we also observed that ifenprodil treatment significantly slows the decay kinetics of the NMDAR-EPSC in a pure GluN1/GluN2B population (Figure 3B and Figure S3B), consistent with the reported ifenprodil-induced decrease in glutamate dissociation rate (Kew et al., 1996). While the longer decay lengthens the envelope of charge transfer, the 70%–80% decrease in peak NMDAR-EPSC amplitude (Figure 3A) has a greater impact on the total charge transfer (Figure 3B; Figure S3B).

In the forebrain, NMDAR-EPSC decay time becomes more rapid during early postnatal development, reflecting an increased contribution of GluN2A subunits with an accompanying reduction of synaptic GluN2B (Flint et al., 1997; Kirson and Yaari, 1996; Sheng et al., 1994). Using the decay kinetics for pure diheteromeric populations of NMDARs, we characterized the time course of the developmental speeding of NMDAR-EPSCs in WT CA1 pyramidal neurons. As shown in Figure 3C, as early as P4 (the earliest age we could obtain reliable EPSCs), mouse CA1 pyramidal cell NMDAR-EPSCs already decay faster than pure GluN1/GluN2B cells and the EPSC speeding is completed by the fifth week. A number of conclusions can be made from these data. First, adult CA1 pyramidal cell NMDAR-EPSCs decay more slowly (the asymptote of a nonlinear regression of the decay time course is 166.1 ± 12.9 msec, Figure S3C) than a pure population of GluN1/GluN2A, suggesting that there is not a complete switch from GluN2B to GluN2A subunits. Interestingly, in layer 2/3 pyramidal neurons of the mouse somatosensory barrel cortex, the switch seems to be more complete than in either mouse or rat CA1 pyramidal cells (Figure 3C). Using the time course of NMDAR-EPSC decay kinetics, we have estimated the percent contribution of GluN2A and GluN2B subunits to the NMDAR-EPSC over development (Figure 3F, solid lines). Importantly, this model makes the assumption that triheteromeric receptors consisting of GluN1/GluN2A/GluN2B have decay kinetics intermediate between diheteromeric receptors, as has been suggested previously (Vicini et al., 1998), but which remains to be conclusively validated. Additionally, based on the estimated open probabilities from Figure 2 of 0.39 for GluN1/GluN2A and 0.21 for GluN1/GluN2B, we have calculated an approximation of the total synaptic GluN2 subunit expression throughout development (Figure 3F, dashed lines), with roughly 65% GluN2A subunits and 35% GluN2B subunits at adult CA1 pyramidal cell synapses.

When ifenprodil is applied to a mixed population of GluN2A- and GluN2B-containing NMDARs, the NMDAR-EPSC decay would be expected to quicken as GluN2B subunits are blocked and the GluN2A contribution is exposed. Simple modeling of this postifenprodil quickening of NMDAR-EPSCs would predict that, in the presence of purely diheteromeric populations, this effect should be greatest when there are equal proportions of GluN2A and GluN2B (Figure S3D). However, the postifenprodil speeding of NMDAR-EPSC decay is only apparent early in postnatal development when GluN2B subunits are predominant (Figure 3C), an observation that has been alluded to previously (Bellone and Nicoll, 2007; Mierau et al., 2004). This observation is further confounded by the slowing of the decay (Figure 3B) from the remaining 20% of current from GluN2B-containing receptors (Figure 3A). One possible explanation is that, in early development, GluN2A subunits are initially expressed as GluN1/GluN2A diheteromers that might be expected to be more exposed after ifenprodil than GluN2A subunits that are part of a triheteromeric receptor. To examine this discrepancy, we attempted to slightly enrich the synaptic population of diheteromeric GluN1/GluN2A by looking at the postifenprodil speeding of NMDAR-EPSCs in ΔGluN2B mice on postnatal days 4 and 5 after P0 Cre injection. We predicted that the postifenprodil speeding of the NMDAR-EPSC decay kinetics would be more pronounced if there was a small enrichment of GluN2A diheteromers. As Cre-mediated gene deletion after P0 virus injection follows a probabilistic time course over the first 7 days (Kaspar et al., 2002), by looking at P4-P5 after P0 injection we expected a percentage of cells to have one or both GluN2B genes deleted such that new NMDARs would have an increased likelihood of containing GluN2A subunits, even in the absence of a significant turnover of extant GluN2B subunits. We found that there was a small insignificant speeding of baseline NMDAR-EPSC decay and, as predicted, a more pronounced postifenprodil quickening of the decay (Figure 3D). Interestingly, the early developmental postifenprodil speeding of NMDAR-EPSC decay is more pronounced in the somatosensory cortex (Figure 3C), suggesting a greater proportion of diheteromeric GluN1/GluN2A receptors.

There is compelling evidence for the existence of triheteromeric GluN1/GluN2A/GluN2B receptors in the forebrain (Al-Hallaq et al., 2007; Chazot and Stephenson, 1997; Luo et al., 1997; Sheng et al., 1994). Based on biochemical analyses, estimates of the percentage of NMDARs that are triheteromeric range from as low as 0%–6% (Blahos and Wenthold, 1996; Chazot and Stephenson, 1997) to as high as 50%–60% (Luo et al., 1997) in the rat forebrain. More recently, sequential immunoprecipitation studies of rat hippocampal membranes estimated that 15%–40% of NMDARs are triheteromeric (Al-Hallaq et al., 2007). However, the incomplete understanding of the biophysical and pharmacologic properties of these triheteromeric receptors have made the interpretation of studies using subtype-selective antagonists difficult (Neyton and Paoletti, 2006). Recently though, it has been elegantly demonstrated that in triheteromeric receptors, a single GluN2B subunit is sufficient to confer high ifenprodil affinity, but the maximal level of inhibition by ifenprodil drops to approximately 20% (Hatton and Paoletti, 2005). Here we show that while the NMDAR-EPSC decay kinetics continue to speed up through development, the time course of ifenprodil sensitivity flattens at around 50%–60% after approximately P9 (Figure 3E and Figure S3D), suggesting the presence of a significant amount of synaptic triheteromeric receptors, consistent with a recent report (Rauner and Köhr, 2011). Interestingly, in the somatosensory cortex, there is a more complete switch in ifenprodil sensitivity during development, suggesting fewer triheteromeric receptors in these cells (Figure 3E).

Effects of GluN2 Subunit Deletion on NMDAR-EPSC Amplitude and Charge Transfer

The developmental increase in the GluN2A/GluN2B ratio is bidirectionally influenced by sensory experience (Quinlan et al., 1999; Roberts and Ramoa, 1999), synaptic plasticity (Bellone and Nicoll, 2007), and homeostatic plasticity (Lee et al., 2010). The trafficking, targeting, and degradation of GluN2A and GluN2B are differentially regulated at nearly every level (Yashiro and Philpot, 2008). GluN2A seems to have greater avidity for synapses than GluN2B based on the reduced lateral diffusion (Groc et al., 2006) and endocytosis (Lavezzari et al., 2004) of GluN2A-containing receptors. Indeed, transgenic overexpression of GluN2B in layer 2/3 pyramidal cells in the visual cortex failed to elevate synaptic GluN2B levels (Philpot et al., 2001).

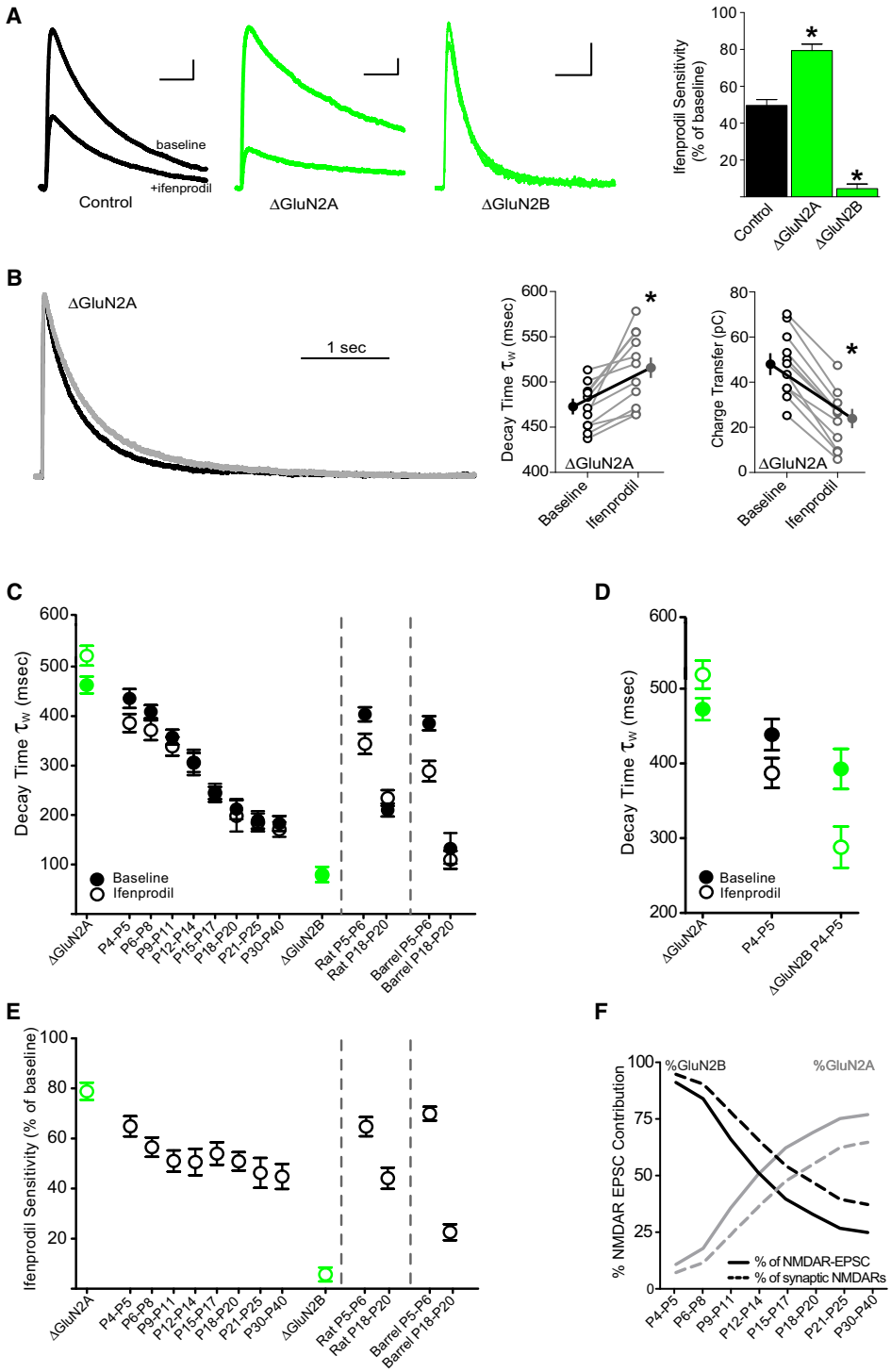

Figure 3. Ifenprodil Sensitivity of Pure Synaptic Diheteromeric NMDARs and the Developmental Time Course of Subunit Switch

(A) Representative-evoked NMDAR-EPSC traces from transfected or control cells from *Grin2b*$^{fl/fl}$ or *Grin2b*$^{fl/fl}$ mice at P18 after P0 injection of rAAV1-Cre-GFP recorded at +40 mV in the presence of 10 μM NBQX. Upper traces are baseline EPSCs, lower traces are 40–50 min after application of 3 μM ifenprodil (scale bars represent 200 msec, 20 pA). Bar graph shows the ifenprodil sensitivity represented as a percent decrease in the peak current (control, 49.1 ± 6.6%, n = 21; ΔGluN2A, 79.3 ± 4.5%, n = 13; ΔGluN2B, 4.5 ± 2.3%, n = 11).

(B) Normalized representative traces from a Cre-expressing neuron *Grin2a*$^{fl/fl}$ mice at baseline (black) and after 40-50 min of 3 μM ifenprodil application (gray). Graphs of individual cells pre- and postifenprodil show an increase in decay time (left, baseline 472.2 ± 7.5, n = 11; postifenprodil 518.1 ± 11.3, n = 11; $p < 0.001$, paired *t*-test) and a decrease in charge transfer (right, baseline 47.9 ± 4.3, n = 11; postifenprodil 23.4 ± 3.8, n = 11; $p < 0.001$, paired *t*-test).

Therefore, we examined the impact of early postnatal deletion of GluN2A or GluN2B subunits on NMDAR trafficking to synapses.

Using paired recordings from GFP-expressing and neighboring control cells allows for rigorous, quantitative study of the postsynaptic effects of the genetic manipulation while controlling for presynaptic inputs. As shown in Figure 4A, P0 deletion of either GluN1 or both GluN2A and GluN2B results in a complete elimination of NMDAR-EPSCs in paired CA1 pyramidal neurons. Single-gene deletion of GluN2A had no effect on NMDAR-EPSC amplitude (Figure 4B), while GluN2B deletion resulted in an approximately 40% reduction in peak EPSC amplitude (Figure 4B). Given the differences in decay kinetics between GluN2A and GluN2B diheteromeric receptors, these differences in peak amplitude would be expected to have large impacts on total charge transfer per EPSCs. Indeed, approximately 1.8-fold more charge was transferred per NMDAR-EPSC in ΔGluN2A cells than control cells (Figure 4C). Conversely, the total charge transfer per NMDAR-EPSCs from ΔGluN2B cells was only about 25% that of control cells (Figure 4C).

GluN2B and GluN2A Deletions Increase AMPAR-EPSCs by Distinct Mechanisms

Due to the significant differences in NMDAR-EPSCs between ΔGluN2A and ΔGluN2B cells, we examined the effects of GluN2 subunit deletion on AMPAR-EPSCs as a means of assessing synaptic strength and function. We have recently shown that late embryonic deletion of GluN1 in CA1 pyramidal neurons increases AMPAR-EPSCs and enhances the number of functional synapses (Adesnik et al., 2008) via a homeostatic-like mechanism (Lu et al., 2011). Similarly, we show here that postnatal deletion of either GluN1 or simultaneous deletion of both GluN2A and GluN2B also results in a significant increase in AMPAR-EPSCs (Figure 5A). Surprisingly, deletion of either GluN2A or GluN2B individually also resulted in a similar increase in AMPAR-EPSCs (Figure 5B). As none of the genetic deletions affected the paired-pulse ratio (Figure 5C), a measure of transmitter release probability, these effects are likely to be postsynaptic in origin. Furthermore, we recently demonstrated that the potentiation of AMPARs after deletion of GluN1 requires the GluA2 subunit (Lu et al., 2011). In agreement, there were no changes in AMPAR-EPSC rectification, a measure of the GluA2 content of AMPARs (Figure 5D), after deletion of GluN2A, GluN2B or both, suggesting that AMPARs trafficked to synapses contain the GluA2 subunit.

Given the unexpected finding that deletion of either GluN2A or GluN2B results in the potentiation of AMPAR-EPSCs, we next asked whether these manipulations may be increasing AMPAR responses by different mechanisms. For instance, the increase in synaptic transmission could be due to enhanced synaptic strength at individual synapses or to a greater number of functional synaptic inputs. To test this, we measured AMPA receptor-mediated, action potential-independent, miniature excitatory postsynaptic currents (mEPSCs) in neighboring Cre-expressing and control cells. We found that deletion of GluN2A resulted in a significant increase in mEPSC amplitude with no significant change in frequency (Figures 6A and 6D), suggesting a strengthening of existing synapses with no apparent change in the number of functional synapses. Conversely, deletion of GluN2B led to an increased frequency of mEPSCs without a change in amplitude (Figures 6B and 6D), suggesting an increase in the number of functional synapses. Deletion of both subunits simultaneously resulted in an expected robust increase in mEPSC frequency and a small significant increase in amplitude (Figures 6C and 6D).

As changes in overall NMDAR expression and activity may contribute to the changes in AMPAR levels, we performed a set of control experiments. First, heterozygous *Grin1*$^{fl/-}$ mice were injected with rAAV1-Cre-GFP at P0. Deletion of GluN1 was previously shown to increase AMPAR-EPSCs and mEPSC frequency (Adesnik et al., 2008). With an approximately 30% reduction of NMDAR-EPSCs in the heterozygous mice, there were no significant changes in AMPAR-EPSCs or mEPSC frequency (Figure S4A). Second, we examined whether removal of the NMDAR protein or its activity is required for the increase in AMPAR-EPSCs and mEPSC frequency. Using organotypic slice culture, in which GluN1 deletion shows the same effect (Adesnik et al., 2008), we have shown no significant changes in mEPSC frequency upon deletion of GluN1 in slices incubated with continuous AP5 (Figure S4B), suggesting that the loss of NMDAR activity, not just the NMDAR protein is responsible for the enhancement of AMPAR responses.

Furthermore, as changes in dendritic spine density or length could effect mEPSC frequency, a detailed examination of neuronal morphology was performed. CA1 pyramidal neurons were filled with fluorescent dye, fixed, and examined with confocal microscopy (Figure 7; Figure S5). There was no significant change in the average number of branch points or lengths of apical or basal dendrites (Figure 7B; Figure S5B). However, while deletion of GluN2A had no effect on spine density, deletion of GluN2B showed a small but significant reduction in both apical and basal spine density (Figure 7A; Figure S5A), similar to previous reports (Akashi et al., 2009; Espinosa et al., 2009; Gambrill and Barria, 2011). Interestingly, as we previously reported (Adesnik et al., 2008), deletion of GluN1 increased mEPSC frequency without any change in dendritic spine density,

(C) Developmental time course of NMDAR-EPSC speeding in mouse and rat CA1 and mouse barrel cortex layer 2/3 pyramidal neurons. Filled symbols represent baseline NMDAR-EPSC decay kinetics, open symbols represent decay kinetics 40–50 min after application of 3 μM ifenprodil. Recordings from *Grin2a*$^{fl/fl}$ or *Grin2b*$^{fl/fl}$ mice included for comparison. Each point represents n = 6–20 cells from at least 3 animals.

(D) Effect of ifenprodil on NMDAR-EPSC decay kinetics after partial removal of GluN2B. Recordings from *Grin2a*$^{fl/fl}$ mice are from P18-P20, and control and *Grin2b*$^{fl/fl}$ mice are from P4-P5.

(E) Developmental time course of NMDAR-EPSC ifenprodil sensitivity, represented as percent decrease in peak current after ifenprodil. Recordings from *Grin2a*$^{fl/fl}$ or *Grin2b*$^{fl/fl}$ mice included for comparison.

(F) Estimated percent contribution of GluN2A and GluN2B subunits to the NMDAR-EPSC over development assuming triheteromeric receptors have intermediate decay kinetics (solid lines). Dashed lines represent the estimated total synaptic GluN2 subunits based on the open probability estimated in Figure 2 (0.39 for GluN1/GluN2A and 0.21 for GluN1/GluN2B). See also Figure S3.

All data represent mean ± SEM.

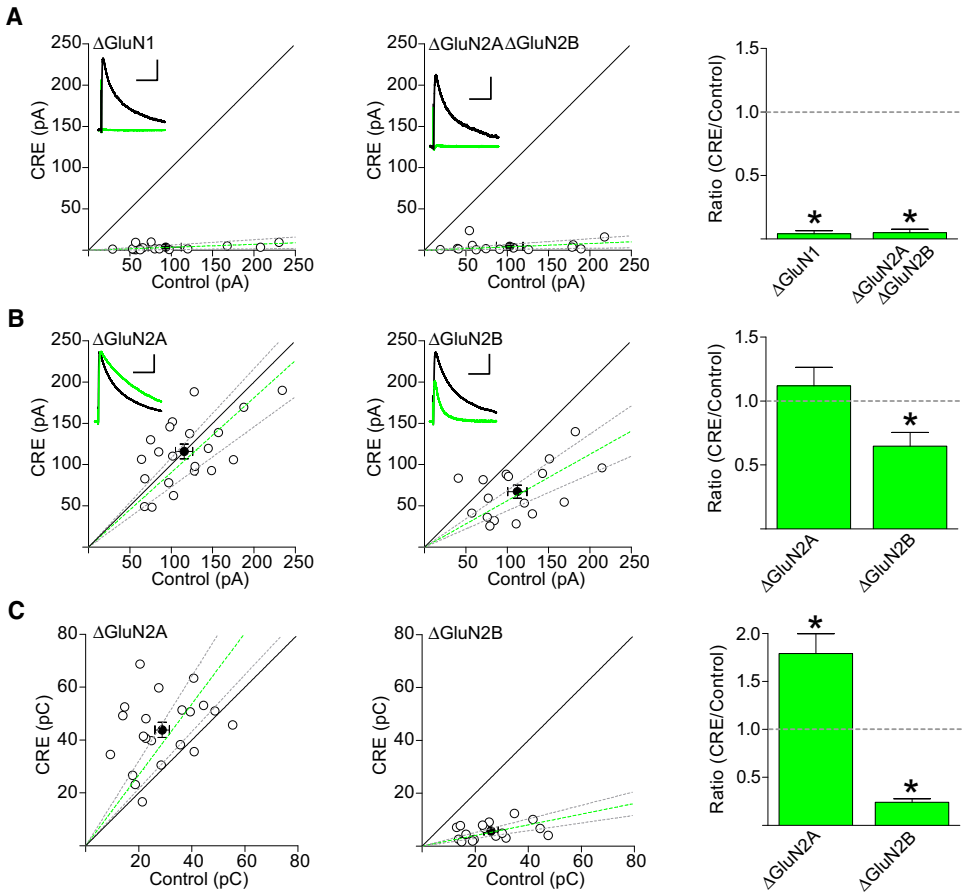

Figure 4. NMDAR-EPSCs after Deletion of GluN2A, GluN2B, or Both

(A–B) Scatter plots of peak amplitudes of evoked NMDAR-EPSCs from single pairs (open circles) and mean ± SEM (filled circles) from transfected and control cells at P16-P25 after P0 injection of rAAV1-Cre-GFP recorded at +40 mV in the presence of 10 μM NBQX. Dashed lines represent linear regression and 95% confidence interval. Sample traces are as follows: control cell, black; transfected cell, green; scale bars represent 100 msec, 25 pA.

(A) *Grin1*$^{fl/fl}$ or *Grin2a*$^{fl/fl}$*Grin2b*$^{fl/fl}$ mice. Bar graph represents the mean ± SEM of the ratios of transfected to control cells from for each pair (ΔGluN1, 0.04 ± 0.02, n = 16, p < 0.001; ΔGluN2AΔGluN2B, 0.05 ± 0.03, n = 15, p < 0.001).

(B) *Grin2a*$^{fl/fl}$ or *Grin2b*$^{fl/fl}$ mice, (ΔGluN2A, 1.11 ± 0.14, n = 21, p = 0.89; ΔGluN2B, 0.65 ± 0.10, n = 17, p = 0.007).

(C) Charge transfer of NMDAR-EPSCs from (B), (ΔGluN2A, 1.79 ± 0.21, n = 21, p < 0.001; ΔGluN2B, 0.24 ± 0.04, n = 17, p < 0.001). Significance determined by Wilcoxon signed-rank test.

which was interpreted as an unsilencing of extant synapses. Thus, the observation that deletion of GluN2B increases mEPSC frequency while causing a reduction in spine density supports a robust unsilencing of synapses.

Given the unusual combination of increased mEPSC frequency with a decrease in dendritic spine density after deletion of GluN2B, we performed a coefficient of variation analysis (Figure 8A) of the evoked AMPAR-EPSCs from Figure 5. This analysis further supports a postsynaptic strengthening after GluN2A deletion and an increase in the number of functional synapses after GluN2B deletion, given that presynaptic release probability was unchanged (see Figure 5C). To more rigorously examine possible changes in the number of silent synapses, we measured the rate of synaptic failures during minimal stimulation (Figures 8B and 8C). Consistent with an unsilencing of synapses, deletion of GluN2B (Figure 8C) decreased synaptic failures, whereas deletion of GluN2A had no effect on the rate of failures (Figure 8B). Furthermore, for both GluN2A and GluN2B deletion, the average amplitude from all trials was significantly increased (Figure 8D), consistent with the increases in AMPAR-EPSC (Figure 5B). However, only GluN2A deletion increased the average amplitude of "nonfailures" (Figure 8E), consistent with the increase in mEPSC amplitude (Figure 6A).

Taken together, our results suggest that deletion of the GluN2B subunit, given its prominent expression in early postnatal development, increases AMPAR-EPSCs by a mechanism similar to the deletion of NMDARs entirely (Adesnik et al., 2008). That is, removing NMDARs during synaptogenesis results in an increase in the number of functional synapses, possibly by removing a silencing signal, without appreciable change in synaptic strength. Early postnatal deletion of GluN2A, however, clearly increases AMPAR-EPSCs by a distinct mechanism

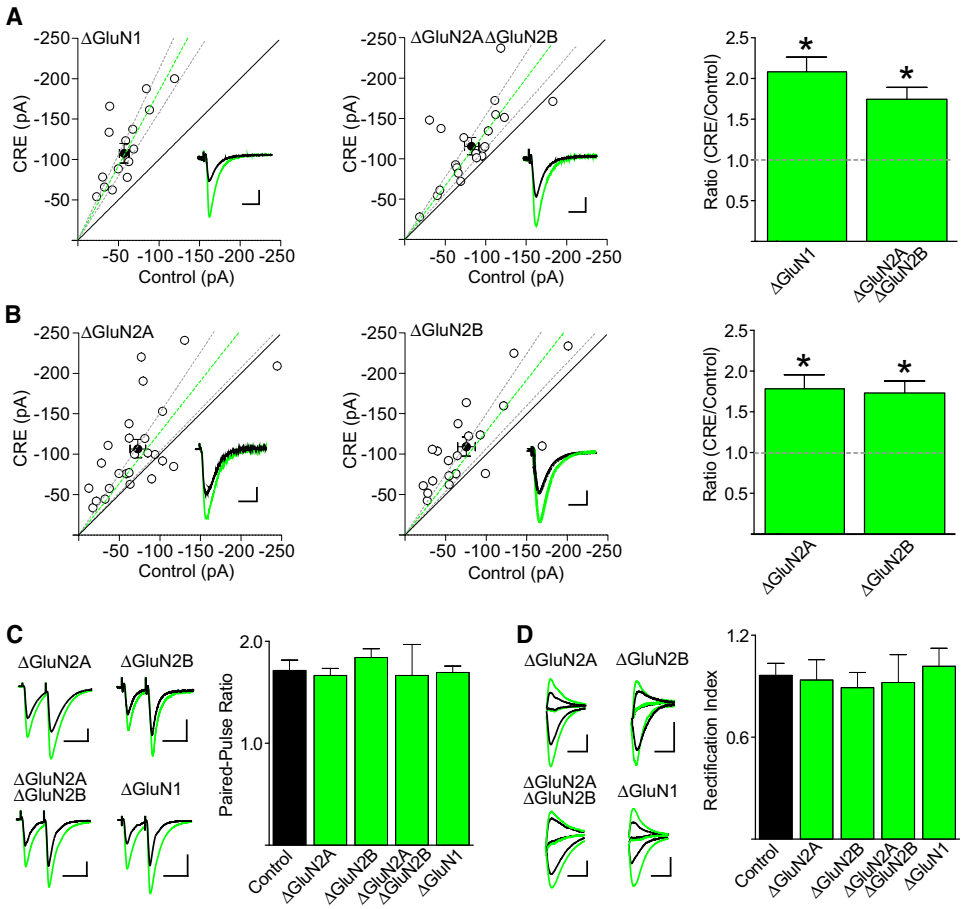

Figure 5. Deletion of GluN2 Subunits Enhances Postsynaptic Excitatory Transmission

(A-B) Scatter plots of the peak amplitudes of evoked AMPAR-EPSCs from single pairs (open circles) and mean ± SEM (filled circles) from transfected and control cells at P16-P25 after P0 injection of rAAV1-Cre-GFP recorded at −70 mV. Dashed lines represent linear regression and 95% confidence interval. Sample traces are as follows: control cell, black; transfected cell, green; scale bars represent 15 msec, 40 pA.

(A) *Grin1*$^{fl/fl}$ or *Grin2a*$^{fl/fl}$*Grin2b*$^{fl/fl}$ mice. Bar graph represents the mean ± SEM of the ratios of transfected to control cells from for each pair (ΔGluN1, 2.09 ± 0.18, n = 15, p < 0.001; ΔGluN2AΔGluN2B, 1.75 ± 0.15, n = 21, p < 0.001). Significance determined by Wilcoxon signed-rank test.

(B) *Grin2a*$^{fl/fl}$ or *Grin2b*$^{fl/fl}$ mice, (ΔGluN2A, 1.78 ± 0.17, n = 25, p < 0.001; ΔGluN2B, 1.72 ± 0.15, n = 20, p < 0.001). Significance determined by Wilcoxon signed-rank test.

(C) Bar graph shows mean ± SEM of the AMPAR-EPSC paired-pulse ratio (control, 1.71 ± 0.10, n = 29; ΔGluN2A, 1.66 ± 0.07, n = 7; ΔGluN2B, 1.84 ± 0.09, n = 15; ΔGluN2AΔGluN2B, 1.66 ± 0.29, n = 8; ΔGluN1, 1.69 ± 0.06, n = 6). Left are representative traces (scale bars represent 15 msec, 40 pA).

(D) Bar graph shows mean ± SEM of the AMPAR-EPSC rectification index recorded in the presence of AP5 (control, 0.96 ± 0.07, n = 19; ΔGluN2A, 0.93 ± 0.12, n = 6; ΔGluN2B, 0.89 ± 0.09, n = 8; ΔGluN2AΔGluN2B, 0.92 ± 0.16, n = 5; ΔGluN1, 1.01 ± 0.11, n = 6). Left are representative traces (scale bars represent 15 msec, 40 pA).

involving an increase in synapse strength without a significant change in the number of functional synapses.

DISCUSSION

We utilized a single-cell genetic approach to address the roles of GluN2A and GluN2B in synapse development. We have recently used this approach to evaluate the composition of AMPAR subunits (Lu et al., 2009) and the role of GluN1 in synapse development, and have shown that this approach reveals cell autonomous effects of the genetic manipulation without competition between neighboring cells (Adesnik et al., 2008). We have shown here, for the first time electrophysiologically, that GluN2A and GluN2B subunits fully account for synaptic NMDAR currents in adult CA1 pyramidal cells. Deletion of GluN2A or GluN2B individually thus allowed for the detailed analysis of pure diheteromeric synaptic populations. The biophysical and pharmacological properties determined for the diheteromeric synaptic NMDARs provided a basis for a detailed characterization of the developmental time course of the NMDAR subunit switch. We found that CA1 pyramidal cell synapses undergo an incomplete subunit switch and express significant amounts of triheteromeric receptors, while sensory cortical neurons undergo a more complete switch from GluN2B to GluN2A. We then evaluated the functional effects of GluN2 subunit deletion on synapse development and found that, similar to GluN1 deletion (Adesnik et al., 2008), deletion of GluN2B subunits increased AMPAR-EPSCs by increasing the number of functional

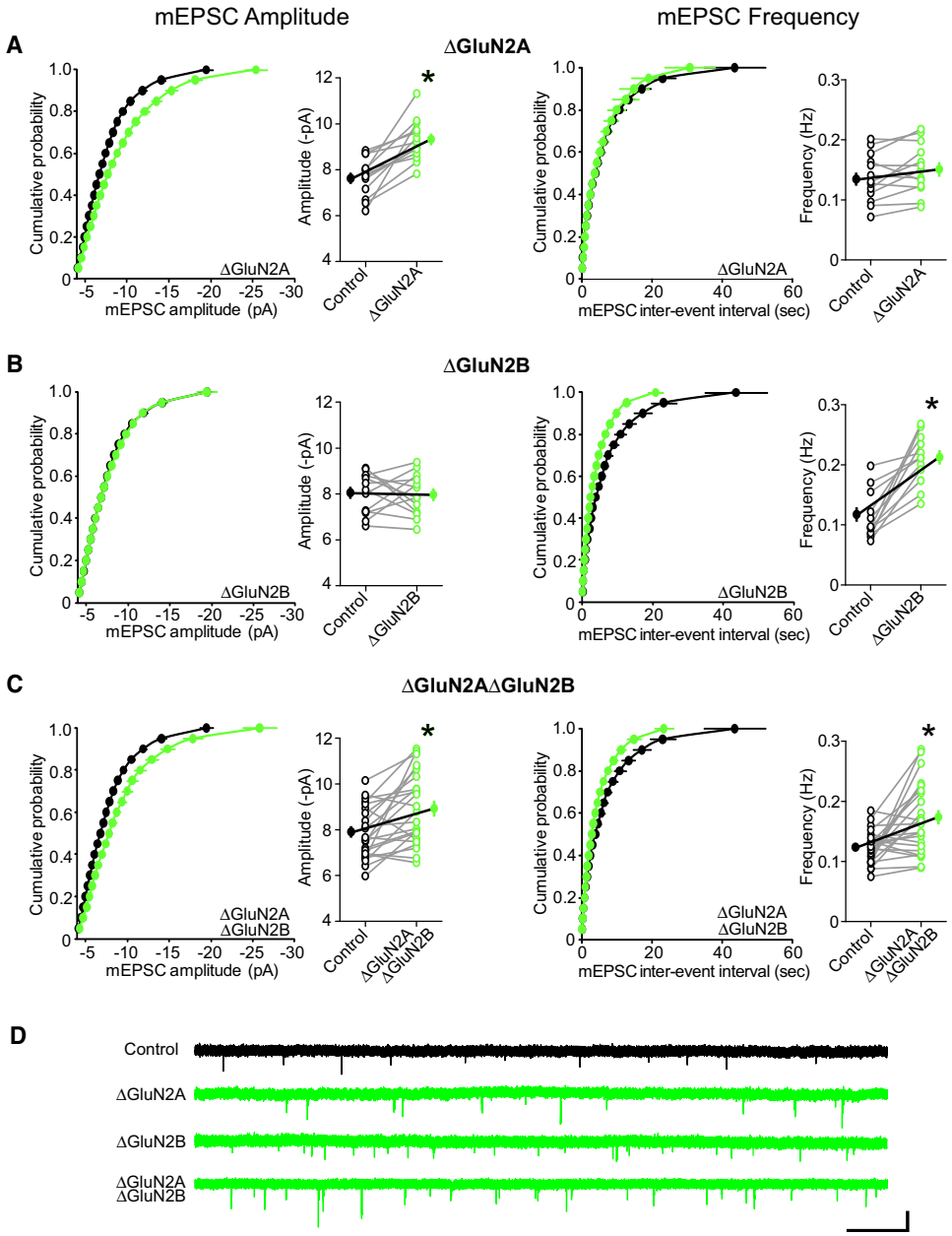

Figure 6. Differential Effects of GluN2 Subunit Deletion on mEPSCs

(A-C) Cumulative distributions and paired average mEPSC amplitudes and inter-event intervals (or frequency) from control (black) and Cre-expressing (green) CA1 pyramidal cells.

(A) *Grin2a*$^{fl/fl}$ mice (mEPSC amplitude: control, 7.69 ± 0.23; Cre, 9.28 ± 0.25; n = 13, p < 0.001; frequency: control, 0.134 ± 0.011; Cre, 0.146 ± 0.012; n = 13, p = 0.059).

(B) *Grin2b*$^{fl/fl}$ mice (mEPSC amplitude: control, 8.01 ± 0.25; Cre, 7.96 ± 0.25; n = 13, p = 0.88; frequency: control, 0.114 ± 0.012; Cre, 0.209 ± 0.012; n = 13, p < 0.001).

(C) *Grin2a*$^{fl/fl}$*Grin2b*$^{fl/fl}$ mice (mEPSC amplitude: control, 7.85 ± 0.24; Cre, 8.94 ± 0.33; n = 24, p < 0.001; frequency: control, 0.123 ± 0.005; Cre, 0.173 ± 0.012; n = 23, p < 0.001).

(D) Representative traces: black, control cell; green, CRE-expressing cell as indicated (scale bars represent 10 s, 10 pA). All data represented as mean ± SEM and analyzed by paired *t*-test. See also Figure S4.

synapses. Surprisingly, however, GluN2A deletion also increased AMPAR-EPSCs, but this increase was secondary to a postsynaptic strengthening of unitary connections without affecting the number of functional synapses.

GluN2A and GluN2B Fully Account for the NMDAR-EPSCs in CA1 Pyramidal Cells

While it has long been suspected that CA1 pyramidal cells express primarily GluN2A and GluN2B (Garaschuk et al., 1996;

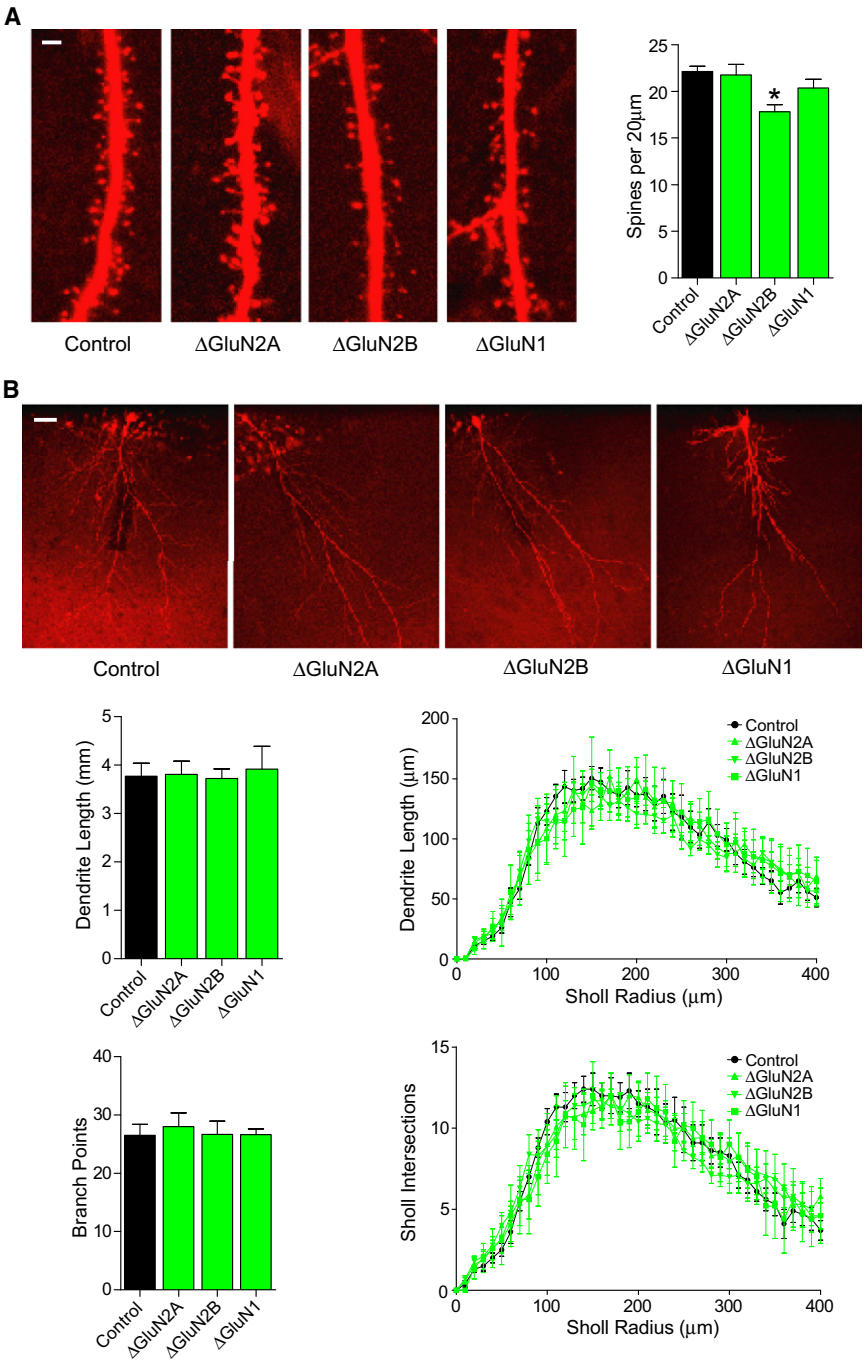

Figure 7. Anatomic Analysis of CA1 Apical Dendrites

(A) Dendritic spines were measured along the primary and secondary apical dendrites at 100–200 μM from the cell body. Representative confocal stacks from control and Cre-expressing cells; scale bar represents 2 μm. Bar graph shows mean spine density (control, 22.14 ± 0.56, n = 13; ΔGluN2A, 21.77 ± 1.12, n = 10, p = 0.76; ΔGluN2B, 17.80 ± 0.78, n = 9, p < 0.001; ΔGluN1, 20.38 ± 0.90, n = 6, p = 0.12; n is the number of neurons). (B) The apical dendritic tree was imaged and analyzed in 3D. Representative confocal stacks from control and Cre-expressing cells; scale bar represents 20 μm. Top bar graph shows mean apical dendrite length (mm) to 400 μm from the cell body (control, 3.77 ± 0.27, n = 8; ΔGluN2A, 3.81 ± 0.27, n = 7; ΔGluN2B, 3.72 ± 0.20, n = 9; ΔGluN1, 3.92 ± 0.47, n = 5). Bottom bar graph shows mean number of branch points to 400 μm from the cell body (control, 26.50 ± 1.88, n = 8; ΔGluN2A, 28.00 ± 2.31, n = 7; ΔGluN2B, 26.67 ± 2.26, n = 9; ΔGluN1, 26.60 ± 0.98, n = 5). Right, Sholl analysis showing no change in overall dendrite length and intersections at 10-μm increments. All data represent mean ± SEM. See also Figure S5.

Watanabe et al., 1992), GluN2C mRNA has been measured in homogenized CA1 region at low levels (Zhong et al., 1995) and GluN2D may also be present (Kirson et al., 1999; Thompson et al., 2002), though it may be localized extrasynaptically (Lozovaya et al., 2004). By using a mouse line with conditional alleles for both GluN2A and GluN2B, we have now shown that by P14 GluN2A and GluN2B subunits fully account for the NMDAR-EPSC in CA1 pyramidal neurons. We cannot, however, exclude a contribution of GluN2C or GluN2D to synaptic currents in neonatal animals as it takes up to a week after injection of Cre virus for recombination to occur in all infected cells (Kaspar et al., 2002). After P14, we have demonstrated, based on rise times, decay kinetics, and ifenprodil sensitivity, that in the ΔGluN2A and ΔGluN2B cells, the NMDAR-EPSCs represent pure diheteromeric receptor populations. These pure diheteromeric populations have characteristics consistent with those measured with fast glutamate application in heterologous systems (Vicini et al., 1998). Furthermore, ifenprodil (3 μM) blocked approximately 80% of synaptic current from a pure synaptic population of GluN1/GluN2B receptors, but had no effect on a pure population of GluN1/GluN2A receptors, similar to findings in heterologous systems (Tovar and Westbrook, 1999).

Using these pure diheteromeric populations, we estimated the subtype dependence of the NMDAR open probability as 0.39 for GluN1/GluN2A receptors, which is approximately two-fold higher than for GluN1/GluN2B diheteromers (0.21). Similar dependence of NMDAR open probability on subunit composition has been shown in heterologous systems (Chen et al., 1999; Erreger et al., 2005), but the results have been less clear in neuronal systems (Chavis and Westbrook, 2001; Prybylowski et al., 2002). Interestingly, the open probability for control cells (0.26), while intermediate, was closer to that of GluN2B diheteromers

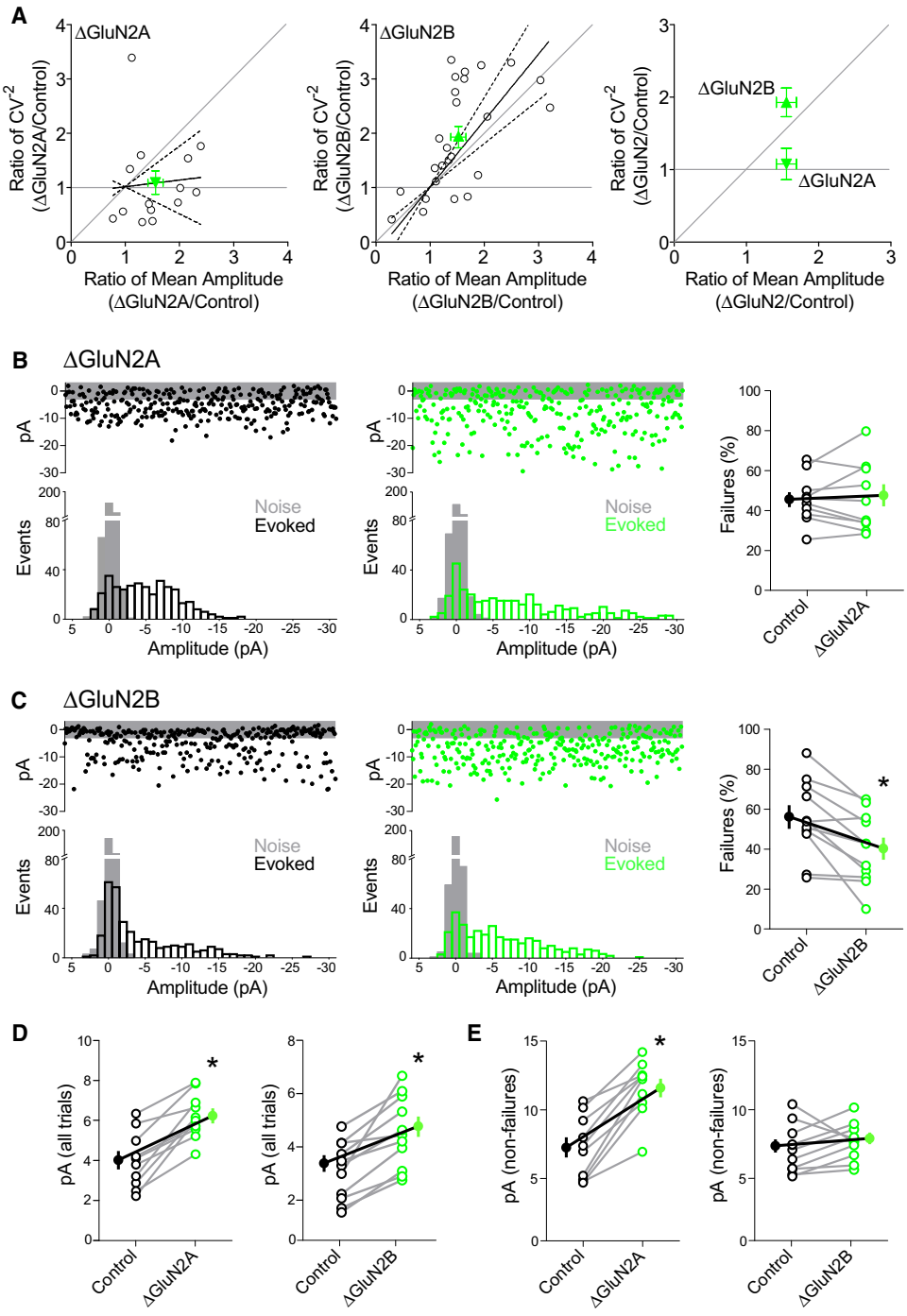

Figure 8. GluN2 Subunits Suppress AMPARs by Distinct Means

(A) Coefficient of variation analysis of AMPAR-EPSCs from paired recordings of control and Cre-expressing cells from *Grin2a*$^{fl/fl}$ or *Grin2b*$^{fl/fl}$ mice. Values above the 45° line suggest increases in quantal content (i.e., number of release sites x presynaptic release probability), whereas values approaching the horizontal line suggest a postsynaptic locus for the increase in AMPAR-EPSC amplitude. Unsilencing of synapses can mimic an increase in the number of release sites when presynaptic release probability is unchanged (see Figure 5C). ΔGluN2A cells (left) show a postsynaptic locus for the increase in AMPAR-EPSC amplitude, whereas ΔGluN2B cells (center) show an increase in quantal content consistent with an unsilencing of synapses. Dashed lines represent linear regression and 95% confidence interval. Summary graph (right) shows the mean ± SEM of the paired sets.

(B and C) Synaptic failures measured during minimal stimulation experiments. Paired recordings of control (left) and Cre-expressing (center, green) cells from *Grin2a*$^{fl/fl}$ (B) or *Grin2b*$^{fl/fl}$ (C) mice. Dots represent the peak evoked response amplitude from repetitive trials, gray bands represent approximate noise threshold. Histograms show the distributions of noise and poststimulus amplitudes. Right: Quantification of synaptic failures in paired recordings; deletion of GluN2B

at a developmental stage when NMDAR decay kinetics are fast, possibly suggesting that triheteromeric NMDARs have an open probability largely influenced by the GluN2B subunit.

GluN2B and GluN2A Differentially Suppress AMPA Receptors at Developing Synapses

Multiple recent studies have shown that inhibiting NMDAR activity early in development increases AMPAR expression and synaptic currents (Adesnik et al., 2008; Grooms et al., 2006; Ultanir et al., 2007), suggesting that NMDAR activity at nascent synapses suppresses the synaptic insertion of AMPARs. We observe here that both GluN2B- and GluN2A-containing NMDARs are involved in the suppression of synaptic AMPAR expression during early postnatal development, albeit by distinct means. Deletion of GluN2B subunits resulted in an increase in AMPAR-EPSCs that is secondary to an increase in mEPSC frequency and a decrease in synaptic failures, without a change in mEPSC amplitude and without an increase in dendritic spine density. This result is consistent with our previous findings with the single-cell deletion of GluN1 (Adesnik et al., 2008) that suggest that baseline signaling through NMDARs in early development suppresses synaptic AMPARs by inhibiting the unsilencing of synapses. Conversely, while the deletion of GluN2A subunits also resulted in an increase in AMPAR-EPSCs, this increase was secondary to an increase in mEPSC amplitude without a significant increase in frequency, suggesting a strengthening of synapses without a change in the number of functional unitary connections. These conclusions were further supported by coefficient of variation and failures analyses. Based on these current and recent results, we suggest the following model (Figure 9): ongoing low-level activity of GluN2B-containing NMDARs early in development limits the constitutive trafficking AMPARs to synapses, perhaps by an LTD-like mechanism. This inhibitory mechanism would ensure that synapses gain AMPARs and mature only after receiving strong or correlated activity, when sufficient calcium enters to drive an LTP-like mechanism. In addition to increasing synaptic AMPARs, strong activity early in young animals (2–9 days old) quickly increases the proportion of synaptic NMDARs that contain GluN2A (Bellone and Nicoll, 2007). This increase in synaptic GluN2A-containing receptors then acts to dampen further synapse potentiation.

It is well established that activation of NMDA receptors can lead to either increases or decreases in synaptic strength depending on the magnitude of the incoming activity (Malenka and Bear, 2004). While many studies have attempted to elucidate specific contributions of GluN2 subunits to different forms of synaptic plasticity in mature neurons, significant controversy remains. Developmentally, however, the ability to induce synaptic plasticity varies as a function of age and experience (Kirkwood et al., 1996; Quinlan et al., 1999; Yashiro and Philpot, 2008). Indeed, the efficacy of LTP induction at thalamocortical synapses decreases after the first postnatal week (Crair and Malenka, 1995; Isaac et al., 1997; Lu et al., 2001), a period that corresponds to the synaptic enrichment in GluN2A subunits. In the visual cortex, the experience-dependent switch between GluN2B- and GluN2A-containing NMDARs (Quinlan et al., 1999) correlates with an increased threshold for inducing LTP (Kirkwood et al., 1996). Thus, it is possible that an increase in GluN2A subunits may decrease the ability to evoke LTP during synapse development. It was recently shown in hippocampal slice culture that the C-terminal tail of GluN2A may directly inhibit LTP (Foster et al., 2010), consistent with earlier work suggesting that the subunit composition, rather than receptor kinetics, correlates with developmental changes in plasticity (Barth and Malenka, 2001). Thus, perinatal removal of GluN2A may remove a brake to further synapse potentiation, leading to the increase in mEPSC amplitude observed here. Consistent with our findings, recordings from CA1 pyramidal cells from transgenic mice expressing GluN2A with its C-terminal tail deleted showed an increase in mEPSC amplitude (Steigerwald et al., 2000).

That GluN2B receptor activity is required for both the maintenance of silent synapses as well as inducing LTP and synapse maturation may initially seem contradictory. However, differences in Ca^{2+} influx during low-level or basal activity versus strong activity may activate different signaling pathways. Indeed, it is well established that an LTP-inducing stimulus can convert AMPAR-silent synapses into AMPAR-signaling synapses (Durand et al., 1996; Isaac et al., 1997; Liao et al., 1995), while, in neonatal neurons, AMPAR silencing can be induced with an LTD-like protocol (Xiao et al., 2004). Our results here suggest that low-level activation of GluN2B-containing NMDARs suppresses AMPAR insertion into synaptic sites, possibly through an LTD-like mechanism at developing hippocampal neurons. Taken together, these observations demonstrate a fundamental developmental role for the NMDA receptor subunit switch in tightly regulating AMPAR recruitment at multiple levels.

Due to the perinatal lethality of the germline GluN2B KO, many groups have recently examined the effects of more selective GluN2B deletion. For example, dissociated cortical cultures from GluN2B KO mice showed an increase in mEPSC amplitude (Hall et al., 2007), in contrast to our findings, though frequency appeared to increase but was not reported. In addition, RNA interference (RNAi) was used to block GluN2B expression with similar effects; however, this manipulation resulted in a complete loss of all NMDAR current (Hall et al., 2007). This discrepancy may be related to the high excitatory drive of dissociated cultures, direct or indirect off-target effects of the GluN2B RNAi on GluN2A expression, or it may suggest that their experimental system may not be broadly generalizable to synapses developing in intact networks. Interestingly, deletion of GluN2B

(C, control 55.4 ± 5.7%, ΔGluN2B 40.32 ± 5.3%, n = 11, $p < 0.01$) but not GluN2A (B, control 45.9 ± 3.8%, ΔGluN2A 46.4 ± 5.4%, n = 10, $p = 0.85$) results in a reduction in synaptic failures.

(D) Average EPSC amplitude from all trials (including failures) shows increased amplitude from both *Grin2A*$^{fl/fl}$ (left, control 4.00 ± 0.44, ΔGluN2A 6.22 ± 0.37, n = 10, $p < 0.001$) and *Grin2b*$^{fl/fl}$ (right, control 3.10 ± 0.33, ΔGluN2B 4.54 ± 0.40, n = 11, $p < 0.001$) mice.

(E) Average EPSC amplitude only from "nonfailures" shows increased amplitude only from *Grin2a*$^{fl/fl}$ (left, control 6.94 ± 0.74, ΔGluN2A 11.95 ± 0.71, n = 10, $p < 0.001$) but not *Grin2b*$^{fl/fl}$ (right, control 7.12 ± 0.51, ΔGluN2B 7.69 ± 0.39, n = 11, $p = 0.23$) mice. All data represented as mean ± SEM and analyzed by paired t test.

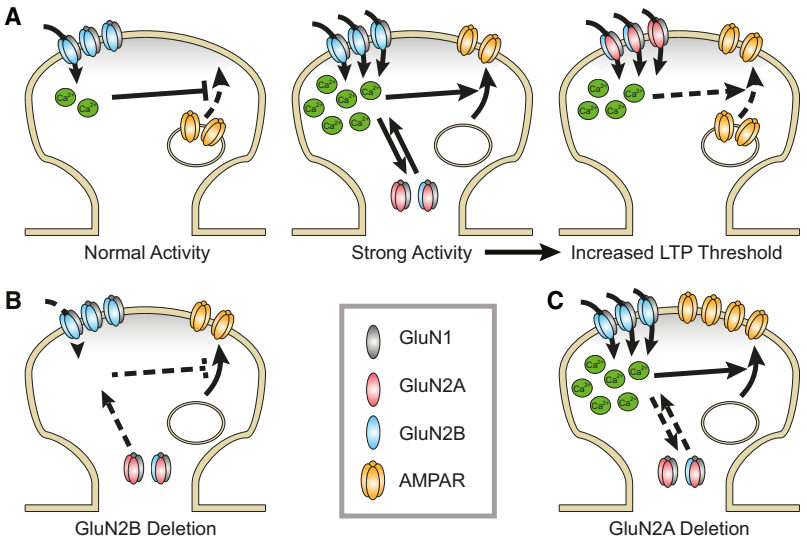

Figure 9. Model for the Role of GluN2 Subunits in Synaptic Maturation

(A) During early postnatal development, modest activity through predominantly GluN2B-containing NMDARs at silent synapses (Adesnik et al., 2008) prevents the constitutive trafficking of AMPARs (Lu et al., 2011) to the postsynaptic density (PSD). This mechanism ensures that synapses only become functional after strong or correlated activity, when enough calcium enters to override the inhibitory pathway and drive AMPAR insertion (possibly via an LTP-like mechanism). This strong activity during early development also triggers the rapid switch from predominantly GluN2B-containing to predominantly GluN2A-containing NMDARs (Bellone and Nicoll, 2007). The increase in GluN2A subunits subsequently raises the threshold for further potentiation of AMPARs.

(B) When GluN2B subunits are deleted during early postnatal development, the inhibitory "silencing" signal is absent, and AMPARs constitutively traffic to the PSD, similar to the deletion of GluN1 (Adesnik et al., 2008).

(C) When GluN2A subunits are deleted, strong activity through GluN2B-containing NMDARs drives synaptic AMPAR insertion, but there is no switch to GluN2A-containing NMDARs. In the absence of the NMDAR subunit switch, further AMPAR potentiation occurs unimpeded.

in the adult hippocampus had no effect on mEPSC amplitude or frequency (von Engelhardt et al., 2008), suggesting a purely developmental effect.

Due to the increase in mEPSC frequency after deletion of GluN2B, we analyzed dendritic anatomy and spine density and saw no significant changes in overall dendrite branching or length in any of the conditions. Previous reports of GluN2 subunit effects on dendritic arborization have revealed subtle changes in dendritic arbor growth and patterning, but not significant changes in overall length (Espinosa et al., 2009; Ewald et al., 2008). We did, however, observe a small significant decrease in spine density with the deletion of GluN2B. This reduction in spines after the deletion of GluN2B has been reported previously (Akashi et al., 2009; Espinosa et al., 2009; Gambrill and Barria, 2011) and may be related to the unfettered early expression of GluN2A (Gambrill and Barria, 2011), as deletion of GluN1 does not alter spine density (Figure 7; Figure S5) (Adesnik et al., 2008). Our conflicting finding that early postnatal GluN2B deletion increases mEPSC frequency similar to GluN1 deletion (Adesnik et al., 2008), but reduces spine density, suggests a functional dissociation of the synapse unsilencing and spine maintenance. Indeed, GluN1 deletion has been shown to increase the motility of spines and ultimately destabilize spines, without significantly affecting spine formation, growth, or expression of synaptic AMPARs (Alvarez et al., 2007). Thus, our current interpretation of these results is that, even with a small loss of spines upon deletion of GluN2B, the increase in mEPSC frequency suggests a robust unsilencing of extant synapses.

On Triheteromeric Receptors and Their Significance

Using the decay kinetics from the pure population of diheteromeric synaptic NMDARs, we provided a detailed time course of the change in NMDAR-EPSC kinetics and ifenprodil sensitivity through the development of mouse CA1 pyramidal cell synapses. Our results suggest the presence of a significant degree of synaptic triheteromeric NMDARs, in agreement with biochemical studies (Al-Hallaq et al., 2007; Luo et al., 1997; Sheng et al., 1994) and physiologic and pharmacologic studies (Tovar and Westbrook, 1999; Rauner and Köhr, 2011). Furthermore, our results provide indirect yet compelling evidence that GluN2A subunits expressed in early postnatal development may initially be diheteromeric, only forming a significant number of triheteromers with GluN2B after P9. Although triheteromeric NMDARs have been conclusively observed in outside-out patches (Momiyama, 2000), direct synaptic analysis has been inconclusive (Lozovaya et al., 2004). Indeed, our results here only provide indirect evidence of synaptic triheteromeric receptors on the basis of their significantly reduced ifenprodil sensitivity (Hatton and Paoletti, 2005). Decay kinetics may be too crude to detect unique properties of triheteromeric receptors, one subunit may dominate the decay kinetics, or channel properties may change as the composition of the postsynaptic density changes. Nevertheless, the more complete switch in ifenprodil sensitivity in layer 2/3 pyramidal cells in the somatosensory cortex compared with CA1 pyramidal cells suggests a key difference between these brain regions. Similarly, NMDAR-EPSCs in the adult prefrontal cortex remain significantly more sensitive to ifenprodil compared with the V1 visual cortex (Wang et al., 2008). Alternative explanations include GluN1 splice variant expression or the presence of GluN3 subunits. GluN1 splice variants, however, have been shown to not significantly influence NMDAR decay kinetics (Vicini et al., 1998) or ifenprodil sensitivity (Gallagher et al., 1996). The brief developmental expression of GluN3 subunits is an intriguing possibility (Wong et al., 2002). GluN3 subunits likely form triheteromeric complexes with two GluN1 subunits and one GluN2 subunit (Al-Hallaq et al., 2002), and there is recent evidence for synaptically expressed GluN3A (Roberts et al., 2009). While the biophysical properties of synaptic GluN1/GluN2A/GluN3 triheteromers, for example, are unknown, one might anticipate

them to have the rapid EPSC decay and low ifenprodil sensitivity similar to GluN2A-containing diheteromers, which would be consistent with our early developmental findings.

What might be the function of synaptic triheteromeric receptors? There is evidence that NMDAR subunit composition may be tailored to meet the needs of a particular neuron or pathway (Ito et al., 1997; Kumar and Huguenard, 2003). Triheteromeric receptors may either represent an intermediate between more pure diheteromeric populations or impart unique properties to the synapse. Additionally, triheteromeric receptors may be a way for synapses to maintain a significant proportion of GluN2B subunits, possibly to provide a greater allowance for bidirectional plasticity. As GluN2A subunits seem to have a greater avidity for synapses than GluN2B subunits, complexing GluN2B subunits with GluN2A subunits may provide a cellular mechanism for maintaining the stable synaptic presence of GluN2B. Indeed, as GluN2B in synapses promotes the recruitment of GluN2B-binding proteins such as CaMKII (Leonard et al., 1999), triheteromeric receptors might provide a unique mix of precise coincidence detection and scaffolding of key mediators of plasticity within a single receptor complex.

EXPERIMENTAL PROCEDURES

Electrophysiology

Acute transverse 300-μm hippocampal slices were prepared and simultaneous dual whole-cell recordings and data analysis were performed as described in the Supplemental Experimental Procedures. All paired recordings involved simultaneous whole-cell recordings from one GFP-positive neuron and a neighboring GFP-negative neuron. Recordings were obtained at room temperature with NMDAR-EPSCs obtained at +40 mV (except where indicated) in the presence of 10 μM NBQX and AMPAR-EPSCs obtained at −70 mV. For MK801 experiments, NMDAR-EPSCs before and after application of 40 μM MK801 were fitted to a five-state NMDAR gating model as described in the Supplemental Experimental Procedures. For ifenprodil experiments, 3 μM ifenprodil was applied until an asymptote was achieved, generally 30–40 min with BAPTA in the intracellular solution to prevent Ca^{2+}-mediated effects during extended recordings (Bellone and Nicoll, 2007). TTX (0.5–1 μM) was added to isolate mEPSCs.

Anatomy and Imaging

CA1 pyramidal cells were filled with Alexa Fluor 568 dye through the patch pipette for approximately 10 min. After filling, slices were fixed, mounted, and scanned with confocal microscopy and analyzed as described in the Supplemental Experimental Procedures.

SUPPLEMENTAL INFORMATION

Supplemental Information includes five figures and Supplemental Experimental Procedures and can be found with this article online at doi:10.1016/j.neuron.2011.08.007.

ACKNOWLEDGMENTS

We thank Susumu Tonegawa (Massachusetts Institute of Technology) for the *Grin1*$^{fl/fl}$ mice. We acknowledge Kirsten Bjorgan and Manual Cerpas for their genotyping assistance and all members of the Nicoll laboratory for their support. J.A.G. is funded by a NARSAD Young Investigator Award and is the NARSAD Hammerschlag Family Investigator. R.A.N. is funded by grants from the National Institute of Mental Health.

Accepted: August 9, 2011
Published: September 21, 2011

REFERENCES

Adesnik, H., Li, G., During, M.J., Pleasure, S.J., and Nicoll, R.A. (2008). NMDA receptors inhibit synapse unsilencing during brain development. Proc. Natl. Acad. Sci. USA *105*, 5597–5602.

Akashi, K., Kakizaki, T., Kamiya, H., Fukaya, M., Yamasaki, M., Abe, M., Natsume, R., Watanabe, M., and Sakimura, K. (2009). NMDA receptor GluN2B (GluR epsilon 2/NR2B) subunit is crucial for channel function, postsynaptic macromolecular organization, and actin cytoskeleton at hippocampal CA3 synapses. J. Neurosci. *29*, 10869–10882.

Al-Hallaq, R.A., Jarabek, B.R., Fu, Z., Vicini, S., Wolfe, B.B., and Yasuda, R.P. (2002). Association of NR3A with the N-methyl-D-aspartate receptor NR1 and NR2 subunits. Mol. Pharmacol. *62*, 1119–1127.

Al-Hallaq, R.A., Conrads, T.P., Veenstra, T.D., and Wenthold, R.J. (2007). NMDA di-heteromeric receptor populations and associated proteins in rat hippocampus. J. Neurosci. *27*, 8334–8343.

Alvarez, V.A., Ridenour, D.A., and Sabatini, B.L. (2007). Distinct structural and ionotropic roles of NMDA receptors in controlling spine and synapse stability. J. Neurosci. *27*, 7365–7376.

Barth, A.L., and Malenka, R.C. (2001). NMDAR EPSC kinetics do not regulate the critical period for LTP at thalamocortical synapses. Nat. Neurosci. *4*, 235–236.

Bellone, C., and Nicoll, R.A. (2007). Rapid bidirectional switching of synaptic NMDA receptors. Neuron *55*, 779–785.

Blahos, J., 2nd, and Wenthold, R.J. (1996). Relationship between N-methyl-D-aspartate receptor NR1 splice variants and NR2 subunits. J. Biol. Chem. *271*, 15669–15674.

Chavis, P., and Westbrook, G. (2001). Integrins mediate functional pre- and postsynaptic maturation at a hippocampal synapse. Nature *411*, 317–321.

Chazot, P.L., and Stephenson, F.A. (1997). Molecular dissection of native mammalian forebrain NMDA receptors containing the NR1 C2 exon: direct demonstration of NMDA receptors comprising NR1, NR2A, and NR2B subunits within the same complex. J. Neurochem. *69*, 2138–2144.

Chen, N., Luo, T., and Raymond, L.A. (1999). Subtype-dependence of NMDA receptor channel open probability. J. Neurosci. *19*, 6844–6854.

Clements, J.D., and Westbrook, G.L. (1991). Activation kinetics reveal the number of glutamate and glycine binding sites on the N-methyl-D-aspartate receptor. Neuron *7*, 605–613.

Colonnese, M.T., Shi, J., and Constantine-Paton, M. (2003). Chronic NMDA receptor blockade from birth delays the maturation of NMDA currents, but does not affect AMPA/kainate currents. J. Neurophysiol. *89*, 57–68.

Colonnese, M.T., Zhao, J.P., and Constantine-Paton, M. (2005). NMDA receptor currents suppress synapse formation on sprouting axons in vivo. J. Neurosci. *25*, 1291–1303.

Crair, M.C., and Malenka, R.C. (1995). A critical period for long-term potentiation at thalamocortical synapses. Nature *375*, 325–328.

Cull-Candy, S.G., and Leszkiewicz, D.N. (2004). Role of distinct NMDA receptor subtypes at central synapses. Sci. STKE *2004*, re16.

Durand, G.M., Kovalchuk, Y., and Konnerth, A. (1996). Long-term potentiation and functional synapse induction in developing hippocampus. Nature *381*, 71–75.

Erreger, K., Dravid, S.M., Banke, T.G., Wyllie, D.J., and Traynelis, S.F. (2005). Subunit-specific gating controls rat NR1/NR2A and NR1/NR2B NMDA channel kinetics and synaptic signalling profiles. J. Physiol. *563*, 345–358.

Espinosa, J.S., Wheeler, D.G., Tsien, R.W., and Luo, L. (2009). Uncoupling dendrite growth and patterning: single-cell knockout analysis of NMDA receptor 2B. Neuron *62*, 205–217.

Ewald, R.C., Van Keuren-Jensen, K.R., Aizenman, C.D., and Cline, H.T. (2008). Roles of NR2A and NR2B in the development of dendritic arbor morphology in vivo. J. Neurosci. *28*, 850–861.

Flint, A.C., Maisch, U.S., Weishaupt, J.H., Kriegstein, A.R., and Monyer, H. (1997). NR2A subunit expression shortens NMDA receptor synaptic currents in developing neocortex. J. Neurosci. *17*, 2469–2476.

Forrest, D., Yuzaki, M., Soares, H.D., Ng, L., Luk, D.C., Sheng, M., Stewart, C.L., Morgan, J.I., Connor, J.A., and Curran, T. (1994). Targeted disruption of NMDA receptor 1 gene abolishes NMDA response and results in neonatal death. Neuron *13*, 325–338.

Foster, K.A., McLaughlin, N., Edbauer, D., Phillips, M., Bolton, A., Constantine-Paton, M., and Sheng, M. (2010). Distinct roles of NR2A and NR2B cytoplasmic tails in long-term potentiation. J. Neurosci. *30*, 2676–2685.

Friedman, H.V., Bresler, T., Garner, C.C., and Ziv, N.E. (2000). Assembly of new individual excitatory synapses: time course and temporal order of synaptic molecule recruitment. Neuron *27*, 57–69.

Gallagher, M.J., Huang, H., Pritchett, D.B., and Lynch, D.R. (1996). Interactions between ifenprodil and the NR2B subunit of the N-methyl-D-aspartate receptor. J. Biol. Chem. *271*, 9603–9611.

Gambrill, A.C., and Barria, A. (2011). NMDA receptor subunit composition controls synaptogenesis and synapse stabilization. Proc. Natl. Acad. Sci. USA *108*, 5855–5860.

Garaschuk, O., Schneggenburger, R., Schirra, C., Tempia, F., and Konnerth, A. (1996). Fractional Ca2+ currents through somatic and dendritic glutamate receptor channels of rat hippocampal CA1 pyramidal neurones. J. Physiol. *491*, 757–772.

Groc, L., Gustafsson, B., and Hanse, E. (2006). AMPA signalling in nascent glutamatergic synapses: there and not there! Trends Neurosci. *29*, 132–139.

Grooms, S.Y., Noh, K.M., Regis, R., Bassell, G.J., Bryan, M.K., Carroll, R.C., and Zukin, R.S. (2006). Activity bidirectionally regulates AMPA receptor mRNA abundance in dendrites of hippocampal neurons. J. Neurosci. *26*, 8339–8351.

Hahm, J.O., Langdon, R.B., and Sur, M. (1991). Disruption of retinogeniculate afferent segregation by antagonists to NMDA receptors. Nature *351*, 568–570.

Hall, B.J., and Ghosh, A. (2008). Regulation of AMPA receptor recruitment at developing synapses. Trends Neurosci. *31*, 82–89.

Hall, B.J., Ripley, B., and Ghosh, A. (2007). NR2B signaling regulates the development of synaptic AMPA receptor current. J. Neurosci. *27*, 13446–13456.

Hatton, C.J., and Paoletti, P. (2005). Modulation of triheteromeric NMDA receptors by N-terminal domain ligands. Neuron *46*, 261–274.

Hestrin, S. (1992). Developmental regulation of NMDA receptor-mediated synaptic currents at a central synapse. Nature *357*, 686–689.

Hsia, A.Y., Malenka, R.C., and Nicoll, R.A. (1998). Development of excitatory circuitry in the hippocampus. J. Neurophysiol. *79*, 2013–2024.

Huettner, J.E., and Bean, B.P. (1988). Block of N-methyl-D-aspartate-activated current by the anticonvulsant MK-801: selective binding to open channels. Proc. Natl. Acad. Sci. USA *85*, 1307–1311.

Isaac, J.T., Crair, M.C., Nicoll, R.A., and Malenka, R.C. (1997). Silent synapses during development of thalamocortical inputs. Neuron *18*, 269–280.

Ito, I., Futai, K., Katagiri, H., Watanabe, M., Sakimura, K., Mishina, M., and Sugiyama, H. (1997). Synapse-selective impairment of NMDA receptor functions in mice lacking NMDA receptor epsilon 1 or epsilon 2 subunit. J. Physiol. *500*, 401–408.

Iwasato, T., Datwani, A., Wolf, A.M., Nishiyama, H., Taguchi, Y., Tonegawa, S., Knöpfel, T., Erzurumlu, R.S., and Itohara, S. (2000). Cortex-restricted disruption of NMDAR1 impairs neuronal patterns in the barrel cortex. Nature *406*, 726–731.

Jahr, C.E. (1992). High probability opening of NMDA receptor channels by L-glutamate. Science *255*, 470–472.

Kaspar, B.K., Vissel, B., Bengoechea, T., Crone, S., Randolph-Moore, L., Muller, R., Brandon, E.P., Schaffer, D., Verma, I.M., Lee, K.F., et al. (2002). Adeno-associated virus effectively mediates conditional gene modification in the brain. Proc. Natl. Acad. Sci. USA *99*, 2320–2325.

Kew, J.N., Trube, G., and Kemp, J.A. (1996). A novel mechanism of activity-dependent NMDA receptor antagonism describes the effect of ifenprodil in rat cultured cortical neurones. J. Physiol. *497*, 761–772.

Kirkwood, A., Rioult, M.C., and Bear, M.F. (1996). Experience-dependent modification of synaptic plasticity in visual cortex. Nature *381*, 526–528.

Kirson, E.D., Schirra, C., Konnerth, A., and Yaari, Y. (1999). Early postnatal switch in magnesium sensitivity of NMDA receptors in rat CA1 pyramidal cells. J. Physiol. *521*, 99–111.

Kirson, E.D., and Yaari, Y. (1996). Synaptic NMDA receptors in developing mouse hippocampal neurones: functional properties and sensitivity to ifenprodil. J. Physiol. *497*, 437–455.

Konnerth, A., Keller, B.U., Ballanyi, K., and Yaari, Y. (1990). Voltage sensitivity of NMDA-receptor mediated postsynaptic currents. Exp. Brain Res. *81*, 209–212.

Kumar, S.S., and Huguenard, J.R. (2003). Pathway-specific differences in subunit composition of synaptic NMDA receptors on pyramidal neurons in neocortex. J. Neurosci. *23*, 10074–10083.

Kutsuwada, T., Sakimura, K., Manabe, T., Takayama, C., Katakura, N., Kushiya, E., Natsume, R., Watanabe, M., Inoue, Y., Yagi, T., et al. (1996). Impairment of suckling response, trigeminal neuronal pattern formation, and hippocampal LTD in NMDA receptor epsilon 2 subunit mutant mice. Neuron *16*, 333–344.

Lavezzari, G., McCallum, J., Dewey, C.M., and Roche, K.W. (2004). Subunit-specific regulation of NMDA receptor endocytosis. J. Neurosci. *24*, 6383–6391.

Lee, M.C., Yasuda, R., and Ehlers, M.D. (2010). Metaplasticity at single glutamatergic synapses. Neuron *66*, 859–870.

Leonard, A.S., Lim, I.A., Hemsworth, D.E., Horne, M.C., and Hell, J.W. (1999). Calcium/calmodulin-dependent protein kinase II is associated with the N-methyl-D-aspartate receptor. Proc. Natl. Acad. Sci. USA *96*, 3239–3244.

Li, Y., Erzurumlu, R.S., Chen, C., Jhaveri, S., and Tonegawa, S. (1994). Whisker-related neuronal patterns fail to develop in the trigeminal brainstem nuclei of NMDAR1 knockout mice. Cell *76*, 427–437.

Liao, D., Hessler, N.A., and Malinow, R. (1995). Activation of postsynaptically silent synapses during pairing-induced LTP in CA1 region of hippocampal slice. Nature *375*, 400–404.

Liao, D., Zhang, X., O'Brien, R., Ehlers, M.D., and Huganir, R.L. (1999). Regulation of morphological postsynaptic silent synapses in developing hippocampal neurons. Nat. Neurosci. *2*, 37–43.

Lozovaya, N.A., Grebenyuk, S.E., Tsintsadze, T.Sh., Feng, B., Monaghan, D.T., and Krishtal, O.A. (2004). Extrasynaptic NR2B and NR2D subunits of NMDA receptors shape 'superslow' afterburst EPSC in rat hippocampus. J. Physiol. *558*, 451–463.

Lu, W., Gray, J.A., Granger, A.J., During, M.J., and Nicoll, R.A. (2011). Potentiation of synaptic AMPA receptors induced by the deletion of NMDA receptors requires the GluA2 subunit. J. Neurophysiol. *105*, 923–928.

Lu, W., Man, H., Ju, W., Trimble, W.S., MacDonald, J.F., and Wang, Y.T. (2001). Activation of synaptic NMDA receptors induces membrane insertion of new AMPA receptors and LTP in cultured hippocampal neurons. Neuron *29*, 243–254.

Lu, W., Shi, Y., Jackson, A.C., Bjorgan, K., During, M.J., Sprengel, R., Seeburg, P.H., and Nicoll, R.A. (2009). Subunit composition of synaptic AMPA receptors revealed by a single-cell genetic approach. Neuron *62*, 254–268.

Luo, J., Wang, Y., Yasuda, R.P., Dunah, A.W., and Wolfe, B.B. (1997). The majority of N-methyl-D-aspartate receptor complexes in adult rat cerebral cortex contain at least three different subunits (NR1/NR2A/NR2B). Mol. Pharmacol. *51*, 79–86.

Malenka, R.C., and Bear, M.F. (2004). LTP and LTD: an embarrassment of riches. Neuron *44*, 5–21.

Mierau, S.B., Meredith, R.M., Upton, A.L., and Paulsen, O. (2004). Dissociation of experience-dependent and -independent changes in excitatory synaptic transmission during development of barrel cortex. Proc. Natl. Acad. Sci. USA *101*, 15518–15523.

Momiyama, A. (2000). Distinct synaptic and extrasynaptic NMDA receptors identified in dorsal horn neurones of the adult rat spinal cord. J. Physiol. *523*, 621–628.

Monyer, H., Burnashev, N., Laurie, D.J., Sakmann, B., and Seeburg, P.H. (1994). Developmental and regional expression in the rat brain and functional properties of four NMDA receptors. Neuron *12*, 529–540.

Monyer, H., Sprengel, R., Schoepfer, R., Herb, A., Higuchi, M., Lomeli, H., Burnashev, N., Sakmann, B., and Seeburg, P.H. (1992). Heteromeric NMDA receptors: molecular and functional distinction of subtypes. Science *256*, 1217–1221.

Neyton, J., and Paoletti, P. (2006). Relating NMDA receptor function to receptor subunit composition: limitations of the pharmacological approach. J. Neurosci. *26*, 1331–1333.

Perin-Dureau, F., Rachline, J., Neyton, J., and Paoletti, P. (2002). Mapping the binding site of the neuroprotectant ifenprodil on NMDA receptors. J. Neurosci. *22*, 5955–5965.

Philpot, B.D., Weisberg, M.P., Ramos, M.S., Sawtell, N.B., Tang, Y.P., Tsien, J.Z., and Bear, M.F. (2001). Effect of transgenic overexpression of NR2B on NMDA receptor function and synaptic plasticity in visual cortex. Neuropharmacology *41*, 762–770.

Prybylowski, K., Fu, Z., Losi, G., Hawkins, L.M., Luo, J., Chang, K., Wenthold, R.J., and Vicini, S. (2002). Relationship between availability of NMDA receptor subunits and their expression at the synapse. J. Neurosci. *22*, 8902–8910.

Quinlan, E.M., Philpot, B.D., Huganir, R.L., and Bear, M.F. (1999). Rapid, experience-dependent expression of synaptic NMDA receptors in visual cortex in vivo. Nat. Neurosci. *2*, 352–357.

Rao, A., and Craig, A.M. (1997). Activity regulates the synaptic localization of the NMDA receptor in hippocampal neurons. Neuron *19*, 801–812.

Rauner, C., and Köhr, G. (2011). Triheteromeric NR1/NR2A/NR2B receptors constitute the major N-methyl-D-aspartate receptor population in adult hippocampal synapses. J. Biol. Chem. *286*, 7558–7566.

Roberts, E.B., and Ramoa, A.S. (1999). Enhanced NR2A subunit expression and decreased NMDA receptor decay time at the onset of ocular dominance plasticity in the ferret. J. Neurophysiol. *81*, 2587–2591.

Roberts, A.C., Díez-García, J., Rodriguiz, R.M., López, I.P., Luján, R., Martínez-Turrillas, R., Picó, E., Henson, M.A., Bernardo, D.R., Jarrett, T.M., et al. (2009). Downregulation of NR3A-containing NMDARs is required for synapse maturation and memory consolidation. Neuron *63*, 342–356.

Sakimura, K., Kutsuwada, T., Ito, I., Manabe, T., Takayama, C., Kushiya, E., Yagi, T., Aizawa, S., Inoue, Y., Sugiyama, H., et al. (1995). Reduced hippocampal LTP and spatial learning in mice lacking NMDA receptor epsilon 1 subunit. Nature *373*, 151–155.

Sheng, M., Cummings, J., Roldan, L.A., Jan, Y.N., and Jan, L.Y. (1994). Changing subunit composition of heteromeric NMDA receptors during development of rat cortex. Nature *368*, 144–147.

Steigerwald, F., Schulz, T.W., Schenker, L.T., Kennedy, M.B., Seeburg, P.H., and Köhr, G. (2000). C-Terminal truncation of NR2A subunits impairs synaptic but not extrasynaptic localization of NMDA receptors. J. Neurosci. *20*, 4573–4581.

Thompson, C.L., Drewery, D.L., Atkins, H.D., Stephenson, F.A., and Chazot, P.L. (2002). Immunohistochemical localization of N-methyl-D-aspartate receptor subunits in the adult murine hippocampal formation: evidence for a unique role of the NR2D subunit. Brain Res. Mol. Brain Res. *102*, 55–61.

Tovar, K.R., and Westbrook, G.L. (1999). The incorporation of NMDA receptors with a distinct subunit composition at nascent hippocampal synapses in vitro. J. Neurosci. *19*, 4180–4188.

Tsien, J.Z., Huerta, P.T., and Tonegawa, S. (1996). The essential role of hippocampal CA1 NMDA receptor-dependent synaptic plasticity in spatial memory. Cell *87*, 1327–1338.

Turrigiano, G.G., Leslie, K.R., Desai, N.S., Rutherford, L.C., and Nelson, S.B. (1998). Activity-dependent scaling of quantal amplitude in neocortical neurons. Nature *391*, 892–896.

Ultanir, S.K., Kim, J.E., Hall, B.J., Deerinck, T., Ellisman, M., and Ghosh, A. (2007). Regulation of spine morphology and spine density by NMDA receptor signaling in vivo. Proc. Natl. Acad. Sci. USA *104*, 19553–19558.

Vicini, S., Wang, J.F., Li, J.H., Zhu, W.J., Wang, Y.H., Luo, J.H., Wolfe, B.B., and Grayson, D.R. (1998). Functional and pharmacological differences between recombinant N-methyl-D-aspartate receptors. J. Neurophysiol. *79*, 555–566.

von Engelhardt, J., Doganci, B., Jensen, V., Hvalby, O., Göngrich, C., Taylor, A., Barkus, C., Sanderson, D.J., Rawlins, J.N., Seeburg, P.H., et al. (2008). Contribution of hippocampal and extra-hippocampal NR2B-containing NMDA receptors to performance on spatial learning tasks. Neuron *60*, 846–860.

Wang, H., Stradtman, G.G., 3rd, Wang, X.J., and Gao, W.J. (2008). A specialized NMDA receptor function in layer 5 recurrent microcircuitry of the adult rat prefrontal cortex. Proc. Natl. Acad. Sci. USA *105*, 16791–16796.

Watanabe, M., Inoue, Y., Sakimura, K., and Mishina, M. (1992). Developmental changes in distribution of NMDA receptor channel subunit mRNAs. Neuroreport *3*, 1138–1140.

Williams, K. (1993). Ifenprodil discriminates subtypes of the N-methyl-D-aspartate receptor: selectivity and mechanisms at recombinant heteromeric receptors. Mol. Pharmacol. *44*, 851–859.

Wong, H.K., Liu, X.B., Matos, M.F., Chan, S.F., Pérez-Otaño, I., Boysen, M., Cui, J., Nakanishi, N., Trimmer, J.S., Jones, E.G., et al. (2002). Temporal and regional expression of NMDA receptor subunit NR3A in the mammalian brain. J. Comp. Neurol. *450*, 303–317.

Xiao, M.Y., Wasling, P., Hanse, E., and Gustafsson, B. (2004). Creation of AMPA-silent synapses in the neonatal hippocampus. Nat. Neurosci. *7*, 236–243.

Yashiro, K., and Philpot, B.D. (2008). Regulation of NMDA receptor subunit expression and its implications for LTD, LTP, and metaplasticity. Neuropharmacology *55*, 1081–1094.

Yasuda, H., Barth, A.L., Stellwagen, D., and Malenka, R.C. (2003). A developmental switch in the signaling cascades for LTP induction. Nat. Neurosci. *6*, 15–16.

Zhong, J., Carrozza, D.P., Williams, K., Pritchett, D.B., and Molinoff, P.B. (1995). Expression of mRNAs encoding subunits of the NMDA receptor in developing rat brain. J. Neurochem. *64*, 531–539.

Neuron, Volume *71*

Supplemental Information

Distinct Modes of AMPA Receptor Suppression at Developing Synapses by GluN2A and GluN2B: Single-Cell NMDA Receptor Subunit Deletion In Vivo

John A. Gray, Yun Shi, Hiroshi Usui, Matthew J. During, Kenji Sakimura, and Roger A. Nicoll

Inventory of Supplemental Information:

Supplemental Figure S1, related to Figure 1

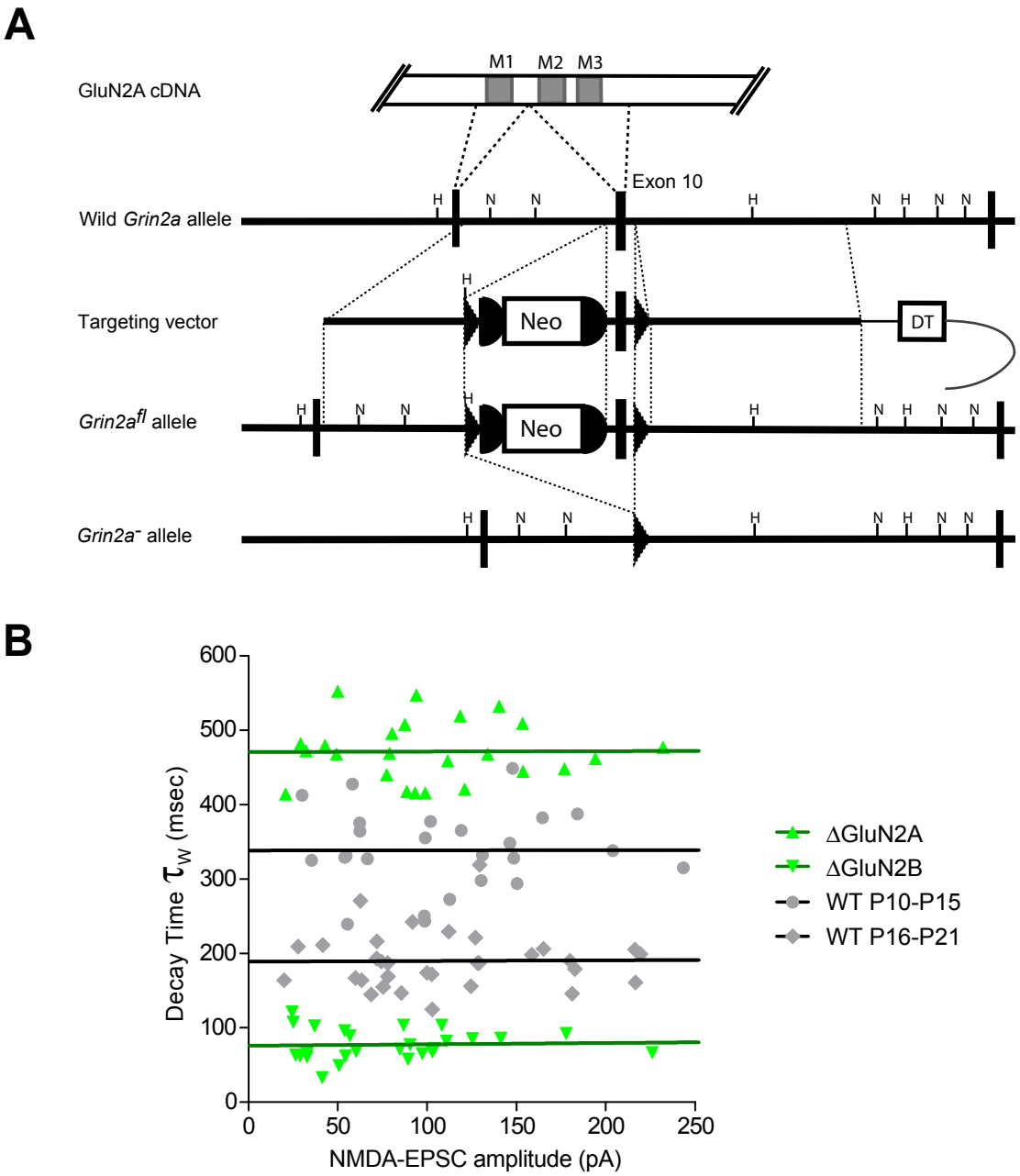

Supplemental Figure S1: Production of GluN2A floxed mice and analysis of space clamp, related to Figure 1.

(A) Production of GluN2A floxed mice by the Cre/loxP system. Schematic representation of cDNA, wild type allele, targeting vector, floxed allele and knockout allele after Cre-mediated recombination. Gray boxes represent the transmembrane segment M1 to M3, while black boxes represent exon sequences, neo cassette (Neo) and diphtheria toxin (DT) cassette. loxP sites indicated by black triangles and frt sites indicated by black semicircles. H, Hind III; N, Nde I.

(B) Analysis of space clamp effectiveness during whole-cell voltage clamp recordings. NMDAR-EPSC decay kinetics were plotted as a function of amplitude for control cells from P10-P15 mice (n=25), P16-P21 mice (n=32) and Cre-expressing cells from *Grin2a*$^{fl/fl}$ (n=24) and *Grin2b*$^{fl/fl}$ (n=26) mice. Linear regression of each data set reveals no significant effect of NMDAR-EPSC amplitude on decay kinetics within 250 pA.

Supplemental Figure S2, related to Figure 2

A

	k_{off}	k_{open}	k_{close}	k_{des}	k_{res}	k_{block}	P_O	$P_{O\,peak}$
Wildtype	4.2 ± 0.8	54.6 ± 6.9	147.3 ± 5.9	5.4 ± 0.6	4.9 ± 2.6	$1.0e^6 \pm 1.7e^5$	0.26 ± 0.02	0.21 ± 0.02
ΔGluN2A	2.5 ± 0.5	28.0 ± 3.3	113.0 ± 10.0	3.0 ± 2.8	4.6 ± 1.6	$1.0e^6 \pm 2.2e^5$	0.21 ± 0.03	0.15 ± 0.02
ΔGluN2B	30.3 ± 3.5	69.0 ± 18.8	105.0 ± 17.0	20.5 ± 4.8	18.6 ± 4.9	$7.1e^5 \pm 1.4e^5$	0.39 ± 0.06	0.28 ± 0.04

B

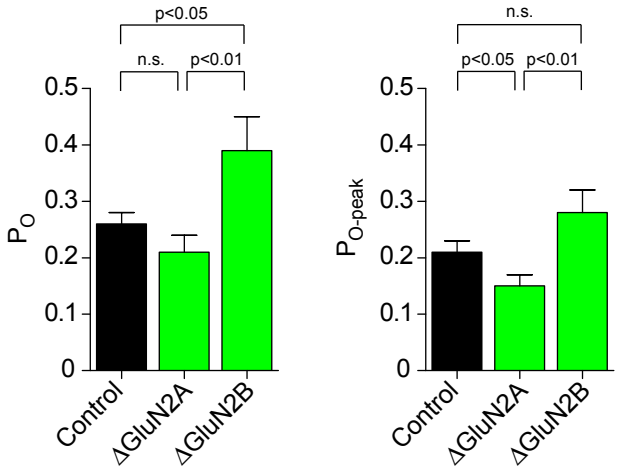

C

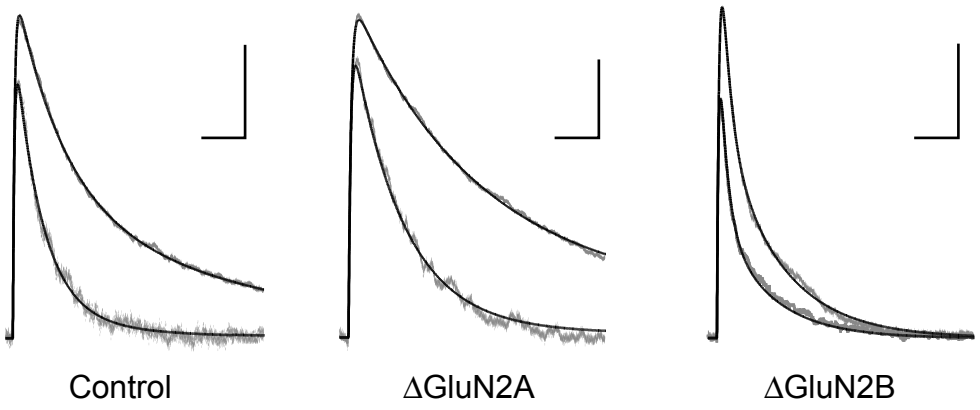

Supplemental Figure S2: Details of open probability estimates, related to Figure 2.

(A) For each experiment, the averaged baseline NMDAR-EPSC and the first EPSC in the presence of MK801 were fitted by a 5-state kinetic model (Figure 2) and the optimized parameters are shown (k_{on} was constrained to 5 $\mu M^{-1}s^{-1}$ (Clements and Westbrook, 1991), data represent mean ± SEM). Open probability (P_O) was calculated as $k_{open}/(k_{open}+k_{close})$ and the peak open probability ($P_{O\text{-}peak}$) was evaluated by dividing the peak currents with the optimal maximal currents.

(B) Bar graphs of P_O and $P_{O\text{-}peak}$. The P_O from ΔGluN2A cells (0.21 ± 0.03, n=11) was significantly lower than from ΔGluN2B cells (0.39 ± 0.06, n=7, p<0.01), while NMDAR-EPSCs from control cells had an intermediate open probability (0.26 ± 0.02, n=10). The $P_{O\text{-}peak}$ from ΔGluN2A cells (0.15 ± 0.02) was also significantly lower than from ΔGluN2A cells (0.28 ± 0.04, p<0.01), while control cells had an intermediate $P_{O\text{-}peak}$ (0.21 ± 0.02).

(C) Representative traces (gray) with fit (black). Scale bars; 40 pA, 100 ms. All data represent mean ± SEM and analyzed by an unpaired Student's t-test.

Supplemental Figure S3, related to Figure 3

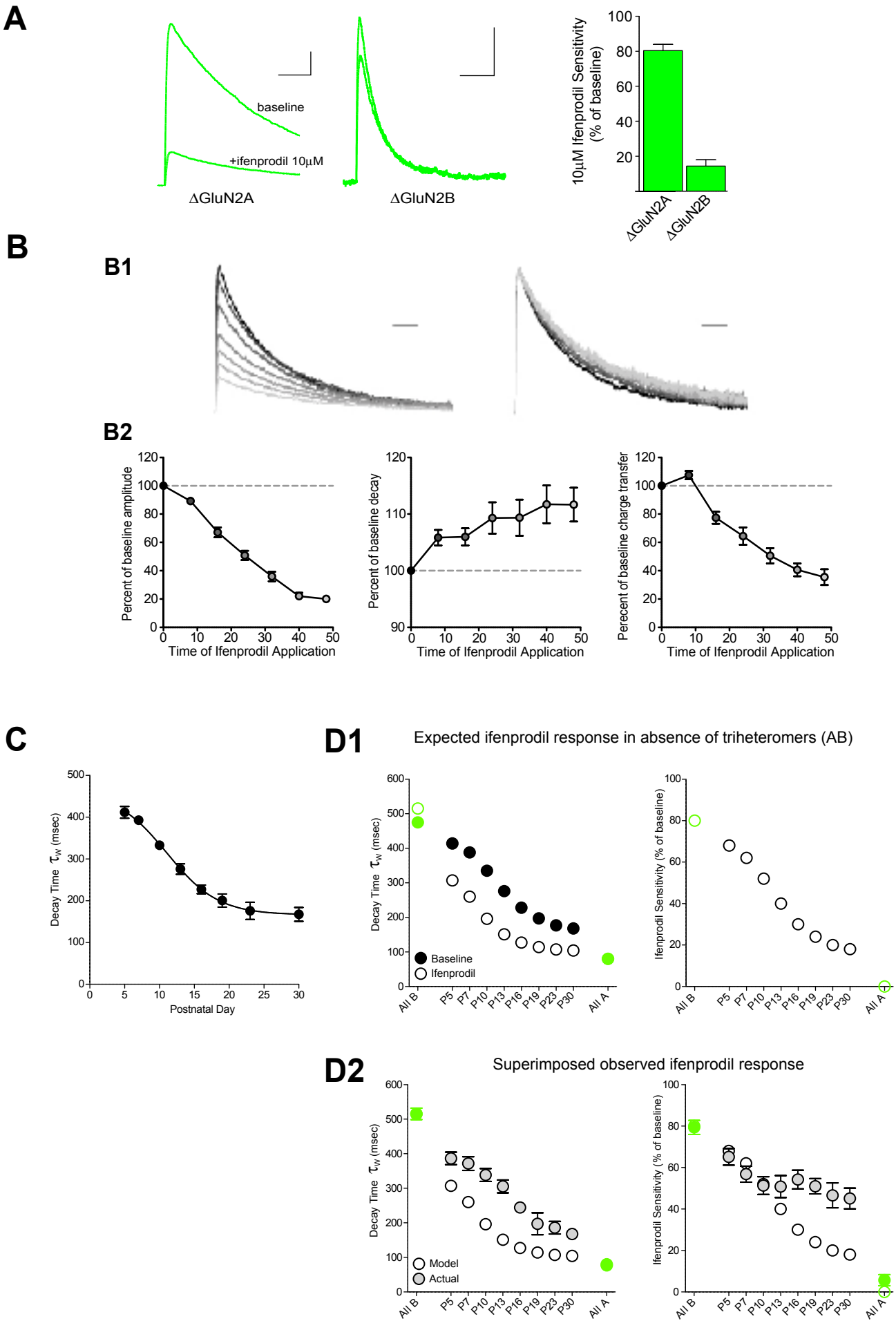

Supplemental Figure S3: Time course of acute ifenprodil inhibition of synaptic GluN1/GluN2B diheteromeric receptors and model of expected developmental response to ifenprodil, related to Figure 3.

(A) Representative NMDAR-EPSC traces from *Grin2a*$^{fl/fl}$ or *Grin2b*$^{fl/fl}$ mice at P18 after P0 injection of rAAV1-Cre-GFP recorded at +40 mV in the presence of 10 μM NBQX. Upper traces are baseline EPSCs, lower traces are 40-50 min after application of 10 μM ifenprodil (scale bars, 200 msec, 20 pA). Bar graph shows the ifenprodil sensitivity represented as a percent decrease in the peak current (ΔGluN2A, 80.5 ± 3.9%, n=4; ΔGluN2B, 14.9 ± 5.4%, n=3). Data represent mean ± SEM.

(B) Time course of changes in NMDAR-EPSCs during application of 3 μM ifenprodil. Whole cell recordings were obtained are from Cre-expressing CA1 pyramidal cells in acute hippocampal slices from P17-P24 *Grin2a*$^{fl/fl}$ mice after P0 injection of rAAV1-Cre-GFP. NMDAR-EPSCs were obtained at +40 mV in the presence of 10 μM NBQX. After obtaining a stable baseline, 3 μM ifenprodil was applied and the NMDAR-EPSCs were averaged in 8 minute intervals. **(B1)** Left, representative traces from a single experiment, baseline in black with lightening grayscale representing time. Right, peak normalized traces. Scale bar is 200 msec. **(B2)** Left, time course of the decrease in peak NMDAR-EPSC amplitude during ifenprodil treatment; data represent mean ± SEM of the baseline normalized amplitude (n=11). NMDAR-EPSC decay lengthens throughout course of ifenprodil treatment, center; data represent mean ± SEM of the baseline normalized decay (n=11). Total charge transfer, right, significantly decreases with ifenprodil treatment, except early in the application; data represent mean ± SEM of the baseline normalized charge transfer (n=11).

(C-D) Model of expected developmental response to 3 μM ifenprodil. **(C)** Time course of the speeding of NMDAR-EPSCs through development in wild-type mouse CA1 pyramidal neurons. NMDAR-EPSCs were obtained at +40 mV in the presence of 10 μM NBQX. Data represent mean ± SEM of all wild-type recordings (note: data in Figure 3A represent only recordings in which ifenprodil data was also obtained). Each point represents n=10-40 cells from at least 3 separate animals. Data was fit with a variable slope non-linear regression (Maximum: 416.4±56.5; Minimum: 166.1±15.8; 50% point: 11.1 days). **(D)** Using the time course of decay kinetics throughout development from **(C)**, we constructed a simple model of the expected ifenprodil response in the absence of triheteromeric receptors. **(D1)** GluN1/GluN2A receptors were given a decay of 80 msec and 0% ifenprodil sensitivity; GluN1/GluN2B receptors were given a baseline decay of 470 msec and 80% ifenprodil sensitivity with a post-ifenprodil decay of 515 msec. Left, post-ifenprodil decay thus represents the decay after removal of 80% of the GluN1/GluN2B current, with the remaining 20% current given a decay time of 515 msec. Right, Expected change in ifenprodil sensitivity in the absence of triheteromeric receptors. **(D2)** Left, the actual post-ifenprodil decay kinetics from Figure 3A superimposed on the simple no-triheteromer model. Right, the actual ifenprodil sensitivity data from Figure 3C superimposed on the simple no-triheteromer model.

Supplemental Figure S4, related to Figure 6

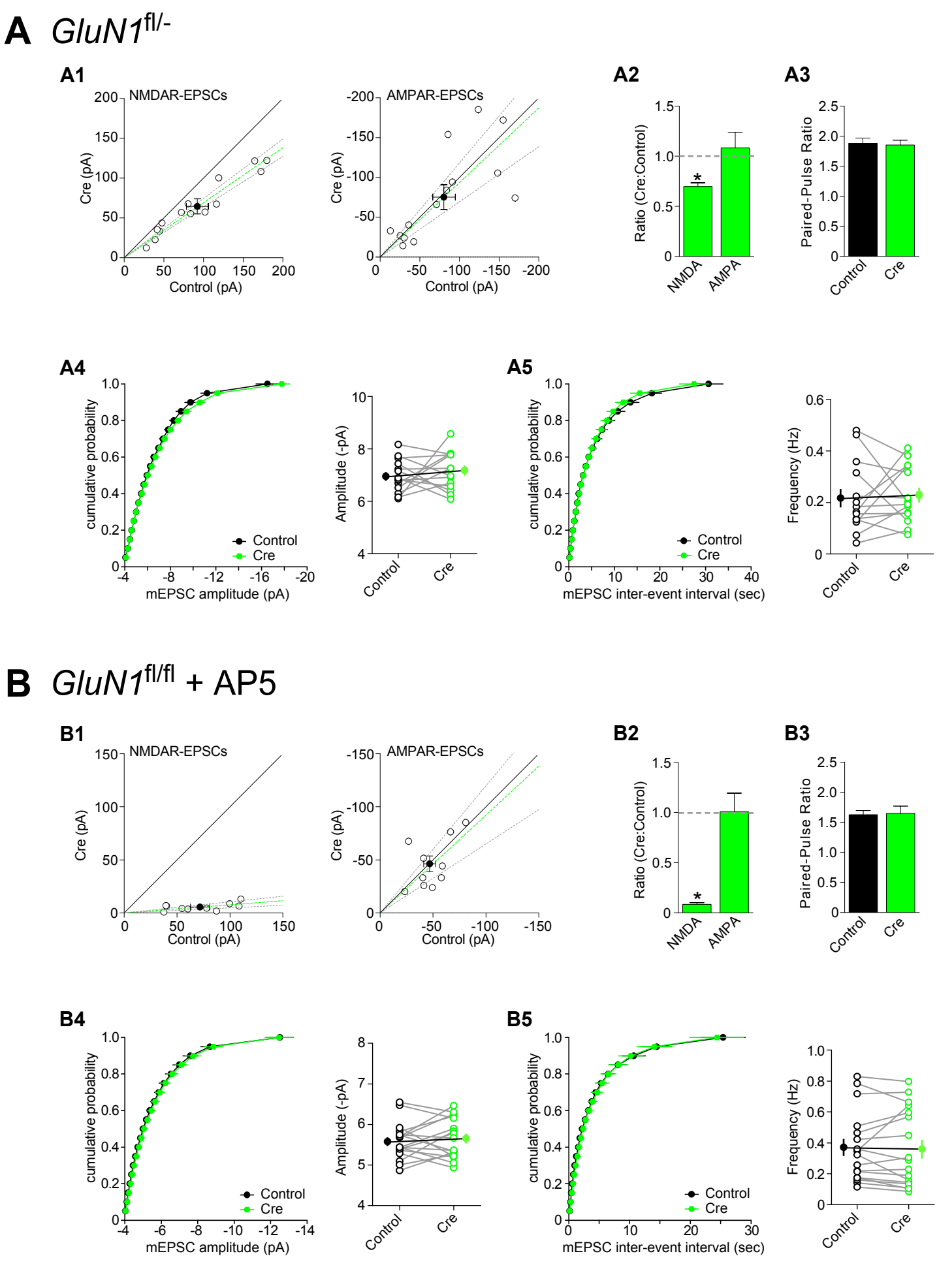

Supplemental Figure S4: Effect of NMDAR expression and activity on AMPAR suppression, related to Fig 6.

(A) *Grin1*$^{fl/-}$ heterozygous mice injected with rAAV1-Cre-GFP at P0 and evoked EPSCs and mEPSCs were recorded from acute hippocampal slices at P16-P22. **(A1)** Scatter plots of peak amplitudes of NMDAR-EPSCs and AMPAR-EPSCs from single pairs (open circles) and mean ± SEM (filled circles) from transfected (Cre) and control cells. Dashed lines represent linear regression and 95% confidence interval. **(A2)** Bar graph shows mean ± SEM of the ratios of transfected to control cells for each pair (NMDAR-EPSCs, 0.69 ± 0.04, n=14, p<0.001; AMPAR-EPSCs, 1.08 ± 0.16, n=14, p=0.60). **(A3)** Bar graph shows mean ± SEM of the AMPAR-EPSC paired-pulse ratio (control, 1.88 ± 0.08, n=14; Cre, 1.86 ± 0.08, n=14; p=0.74). **(A4-A5)** Cumulative distributions and paired average mEPSC amplitudes **(A4)** and inter-event intervals (or frequency) **(A5)** from control (black) and Cre-expressing (green) CA1 pyramidal cells (mEPSC amplitude: control, 6.97 ± 0.17; Cre, 7.15 ± 0.19; n=14, p=0.52; frequency: control, 0.218 ± 0.036; Cre, 0.229 ± 0.029; n=14, p=0.78).

(B) Organotypic hippocampal slice cultures were made from P7 *Grin1*$^{fl/fl}$ mice, biolistically transfected with Cre:GFP, and continuously kept in 40 µM D-AP5 and CA1 pyramidal cells were recorded from DIV20-DIV30. Slices were washed to remove the D-AP5 1-4 hours prior to recording. **(B1)** Scatter plots of peak amplitudes of NMDAR-EPSCs and AMPAR-EPSCs from single pairs (open circles) and mean ± SEM (filled circles) from transfected (Cre) and control cells. Dashed lines represent linear regression and 95% confidence interval. **(B2)** Bar graph shows mean ± SEM of the ratios of transfected to control cells from for each pair (NMDAR-EPSCs, 0.083 ± 0.017, n=10, p<0.001; AMPAR-EPSCs, 1.01 ± 0.19, n=10, p=0.96). **(B3)** Bar graph shows mean ± SEM of the AMPAR-EPSC paired-pulse ratio (control, 1.63 ± 0.07, n=8; Cre, 1.65 ± 0.12, n=8; p=0.81). **(B4-B5)** Cumulative distributions and paired average mEPSC amplitudes **(B4)** and inter-event intervals (or frequency) **(B5)** from control (black) and Cre-expressing (green) CA1 pyramidal cells (mEPSC amplitude: control, 5.59 ± 0.11; Cre, 5.66 ± 0.12; n=17, p=0.50; frequency: control, 0.365 ± 0.055; Cre, 0.364 ± 0.061; n=17, p=0.95). Ratios were analyzed by the Wilcoxon signed rank test and paired mEPSC data were analyzed by a paried Student's t-test.

Supplemental Figure S5, related to Figure 7

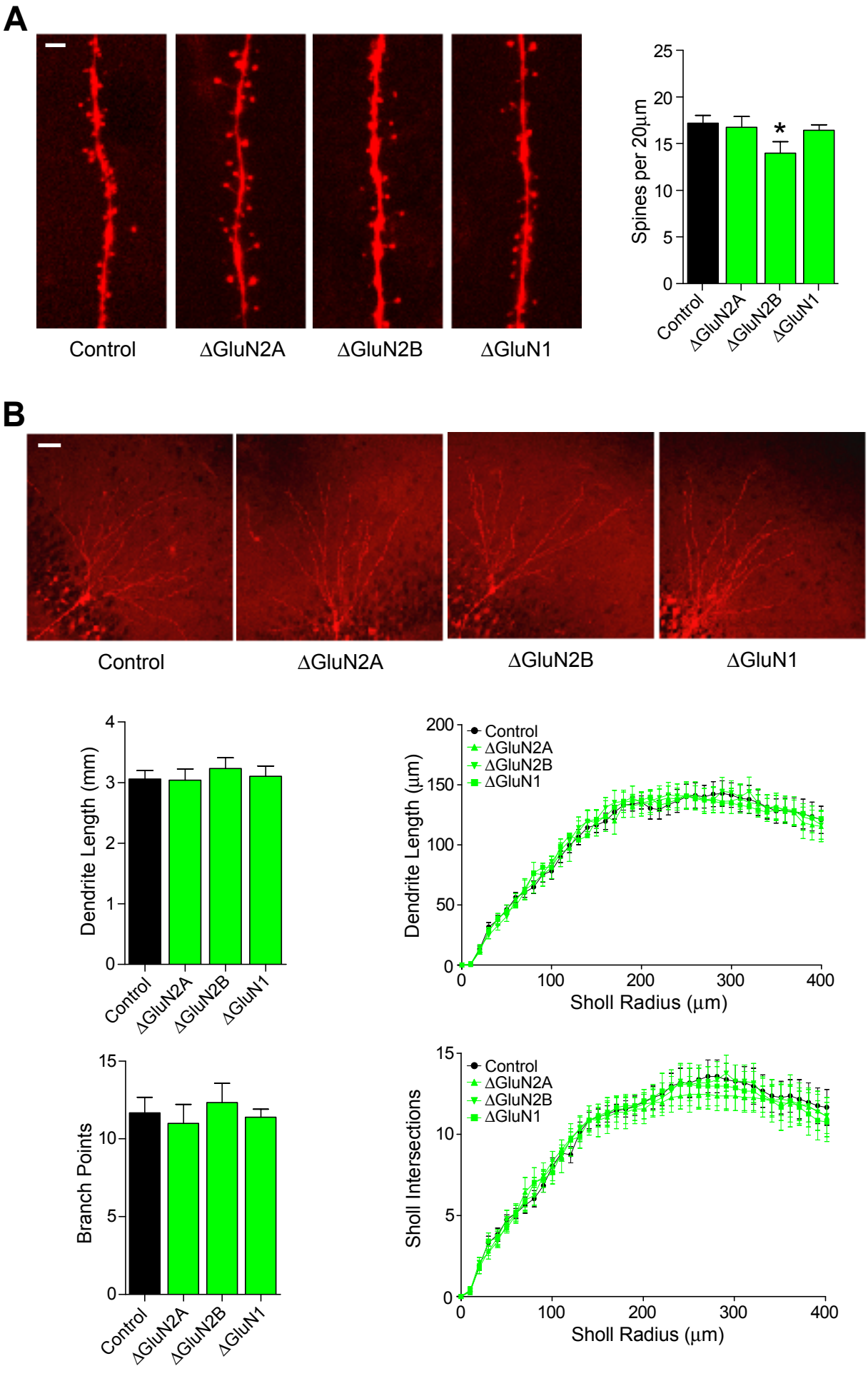

Supplemental Figure S5: Anatomic analysis of CA1 basal dendrites, related to Figure 7.

(A) Dendritic spines were measured along the basal dendrites for 100 μM from the cell body. Representative confocal stacks from Control and Cre-expressing cells; scale bar, 2 μm. Bar graph on right shows mean spine density (control, 17.16 ± 0.81, n=10; ΔGluN2A, 16.73 ± 1.15, n=7, p=0.76; ΔGluN2B, 13.95 ± 1.21, n=8, p=0.04; ΔGluN1, 16.39 ± 0.45, n=6, p=0.12), where n represents the number of neurons from at least two mice. Data represent mean ± SEM and analyzed by Student's t-test.

(B) The basal dendritic tree was imaged and analyzed in 3D. Representative confocal stacks from Control and Cre-expressing cells; scale bar, 20 μm. Top bar graph shows mean basal dendrite length (mm) to 400 μm from the cell body (control, 3.06 ± 0.14, n=12; ΔGluN2A, 3.04 ± 0.19, n=8; ΔGluN2B, 3.23 ± 0.18, n=9; ΔGluN1, 3.11 ± 0.17, n=5). Bottom bar graph shows mean number of branch points to 400 μm from the cell body (control, 11.67 ± 1.00, n=12; ΔGluN2A, 11.00 ± 1.21, n=8; ΔGluN2B, 12.33 ± 1.25, n=9; ΔGluN1, 11.40 ± 0.51, n=5). Right are plots of the Sholl analysis showing overall dendrite length and intersections at 10 μm increments. All data represent mean ± SEM and analyzed by Student's t-test.

Supplemental Experimental Procedures

Mouse Genetics

Animals were housed according to the IACUC guidelines at the University of California, San Francisco. Floxed GluN2A (*Grin2a*$^{fl/fl}$) were produced by homologous recombination using the C57BL/6N strain ES cell line RENKA (Mishina and Sakimura, 2007). A targeting vector was constructed in accordance with mouse genomic DNA databases and contained exon 10 of *Grin2a* gene with 3.8 kb upstream and 5.6 kb downstream homologous genomic DNA fragments and the diphtheria toxin gene for negative selection **(Figure S1)**. A DNA fragment which carried a 34 bp loxP sequence and pgk-1 promoter-driven neomycin phosphotransferase gene (pgk-neo) flanked by two Flp recognition target (*frt*) sites was inserted into the site 216 bp upstream of the exon 10. The other loxP site was introduced into the site 260 bp downstream of the exon 10 in order to eliminate the exon 10 containing the two transmembrane domains (M2 and M3) after Cre-loxP deletion. This resulted in a frame-shift mutation in the *Grin2a* gene **(Figure S1)**. Floxed GluN2B (*Grin2b*$^{fl/fl}$) mice were described previously (Akashi et al., 2009; Mishina and Sakimura, 2007) and were crossed with the floxed GluN2A mice to create *Grin2a*$^{fl/fl}$*Grin2b*$^{fl/fl}$ dual conditional knock-out mice. Gene-targeted *Grin1*$^{fl/fl}$ mice were described previously (Adesnik et al., 2008; Li et al., 1994).

***In Vivo* Postnatal Viral Injection**

Mice were injected at 0-1 days after birth (P0-P1) with high-titer rAAV1-GFP-Cre viral stock (~1-5x10^{12} vg/ml). Newborns were anesthetized on ice for 1.5-2 minutes and then mounted in a custom ceramic mold before being injected with 4.2–9.6 nl of viral solution at nine sites targeting the hippocampus of each cerebral hemisphere by Nanoject (Drummond Scientific) and a beveled glass injection pipette. Pups recovered quickly after injection, were returned to home cage and used for recording 4–40 days afterward. Cre expression was generally limited to the hippocampus with viral infection of a sparse population of CA1 pyramidal cells. Sparse infection of CA3 pyramidal cells was common, though slices with a high density of CA3 pyramidal cell infection were not used.

Slice Preparation and Recording

Transverse 300 µm hippocampal slices were cut from mice on a D.S.K. microslicer DTK-1000 vibrating microtome (Ted Pella, CA) in high sucrose low sodium cutting solution, containing (in mM): KCl 2.5, $CaCl_2$ 0.5, $MgCl_2$ 7, NaH_2PO4 1.25, $NaHCO_3$ 25, glucose 7 and sucrose 210. Freshly cut slices were placed in an incubating chamber containing artificial cerebrospinal fluid (ACSF), containing (in mM) NaCl 119, KCl 2.5, $NaHCO_3$ 26.2, Na_2PO_4 1, glucose 11, $CaCl_2$ 2.5, $MgCl_2$ 1.3, and recovered at 35 °C for ~1h. Slices were then maintained in ACSF at room temperature prior to recording for 0.5-1 h. Slices were then transferred to a submersion chamber on an upright Olympus microscope, perfused in room temperature normal ACSF containing picrotoxin (0.1 mM) and saturated with 95% O2/5% CO2. CA1 pyramidal cells were visualized by infrared differential interference contrast microscopy. The intracellular solution contained (in mM) $CsMeSO_4$ 135, NaCl 8, HEPES 10, Na-GTP 0.3, Mg-ATP 4, EGTA 0.3, QX-314 5, and spermine 0.1. For ifenprodil experiments, 3 µM ifenprodil was applied until an asymptote was achieved, generally 30-40 minutes with BAPTA in the intracellular solution to prevent Ca^{2+}-mediated effects during extended recordings (Bellone and Nicoll, 2007); the intracellular solution contained (in mM) $CsMeSO_4$ 100, BAPTA-tetracesium 10, NaCl 8, HEPES 10, Na-GTP 0.3, Mg-ATP 4, $MgCl_2$ 2.5, and QX-314 5. Cells were recorded with 3- to 5-MΩ borosilicate glass pipettes, following stimulation of Schaffer collaterals with monopolar glass electrodes filled with ACSF placed in stratum radiatum of the CA1 region. Series resistance was monitored and not compensated, and cells in which series resistance varied by 25% during a recording session were discarded. Synaptic responses were collected with a Multiclamp 700B-amplifier (Axon Instruments, Foster City, CA), filtered at 2 kHz, digitized at 10 Hz. GFP positive neurons were identified by epifluorescence microscopy. All paired recordings involved simultaneous whole-cell recordings from one GFP positive neuron and a neighboring GFP negative neuron. The stimulus was adjusted to evoke a measurable, monosynaptic EPSC in both cells. AMPAR-EPSCs were measured at a holding

potential of −70 mV, and NMDAR-EPSCs were measured at +40 mV in the presence of 10 µM NBQX. Paired-pulse ratios were measured by giving two pulses at a 50 ms interval and taking the ratio of the two peaks of the EPSCs from an average of 30–50 sweeps. Rectification indices were calculated as the ratio of the slopes of the two lines connecting average EPSC values at −70 and 0 mV, and, 0 and +40 mV, respectively, in presence of 100 µM APV to block NMDAR-EPSCs. Miniature EPSCs were obtained at −70 mV in the presence of 0.5 µM TTX, 10 µM APV and 0.1 mM picrotoxin. Miniature currents were semi-automatically detected by offline analysis using in-house software in Igor Pro (Wavemetrics) with a detection threshold of 4 pA. For analysis of cumulative distributions, the D'Agostino-Pearson omnibus normality test was used. All paired recording data were analyzed statistically with a two-tailed paired Student's t test. Comparison of paired data groups were performed using the ratios of the GFP-expressing cell to the control cell and analyzed with a Wilcoxon signed-rank test. Linear regressions were obtained using the least squares method. For all other analyses an unpaired two-tailed t-test was used. All errors bars represent standard error measurement.

Estimation of Open Probability

For the MK801 experiments, NMDAR-EPSCs were recorded at +40 mV in the presence of 10 µM NBQX as above. After a stable baseline was obtained, stimulation was stopped and 40 µM MK801 was perfused onto the slices. After 10 minutes, stimulation was restarted. For each experiment, the averaged baseline NMDAR-EPSC and the first EPSC after perfusion of MK801 was fitted to a simplified 5-state NMDAR gating model (Clements and Westbrook, 1991) by simulating synaptic NMDAR currents with a non-restrained strategy (Hessler et al., 1993). In the simulation, a brief pulse of glutamate (1 mM, 1 ms) was delivered and a least squares optimization algorithm was used to find the parameters that optimally fit synaptic currents without MK801. Except for glutamate binding rate (k_{on}) which was constrained to a 5 $\mu M^{-1}s^{-1}$ (Clements and Westbrook, 1991), other parameters were allowed to vary. The simulations were carried out using the SCoP program (Simulation Resources). For each experiment, the first trace recorded in the presence of MK801 was fitted with the parameters acquired from the baseline fitting with the MK801 concentration fixed to 40 µM. The open rate (k_{open}) was allowed to vary since the speeding of current decay is dependent on this rate constant (Rosenmund et al., 1993). In addition, the optimal channel number (the maximal current generated assuming all channels opened simultaneously) and MK801 blocking rate constant were allowed to vary to optimally fit the first current trace in the presence of MK801. The apparent MK801 blocking rate was significantly lower than that experimentally determined in outside-out patches (Jahr, 1992), suggesting that the effective MK801 concentration in the synaptic cleft in acute hippocampal slices is lower than 40 µM.

Coefficient of Variation Analysis

The locus of the increase in AMPAR-EPSC amplitude was estimated by comparing the change in EPSC variance with the change in mean amplitude (Bekkers and Stevens, 1990; Malinow and Tsien, 1990). The coefficient of variation (CV) was calculated as SD/M, where M is the mean EPSC amplitude. The M and SD were measured for a concurrent set of stimuli (40-120 sweeps per pair) from a control and neighboring Cre-expressing cell. It has been shown theoretically and experimentally that changes in CV^{-2} (M^2/SD^2) are independent of quantal size but vary in a predictable manner with quantal content: number of release sites *n* x presynaptic release probability P_r; $CV^{-2} = nP_r/(1-P_r)$ (Bekkers and Stevens, 1990; Del Castillo and Katz, 1954; Malinow and Tsien, 1990; Xiang et al., 1994). Values above the 45° (y=x) line classically suggest increases in quantal content while values approaching the horizontal line (y=1) suggest a postsynaptic locus for the increase in AMPAR-EPSC amplitude. Unsilencing of synapses can mimic an increase in the number of release sites when presynaptic release probability is unchanged (for discussion, see (Kerchner and Nicoll, 2008)). Paired recordings of less than 40 sweeps were excluded. Linear regressions were obtained using the least squares method.

Failures Analysis

Failures analysis was preformed as previously described (Goold and Nicoll, 2010). Briefly, a minimal stimulus was adjusted to yield approximately 50% failures. The number of failures was estimated as double the

number of events with peak currents >0 pA (as AMPAR currents have expected amplitudes <0 pA), and divided by the total number of trials to yield the failure rate for a given cell. The noise distribution was estimated in each cell at 350 ms after the stimulus when any AMPAR EPSC would be expected to have returned to baseline. "Non-failures" were approximated by removing all events with amplitude >0 pA as well as an equal number of the <0 pA events with the lowest absolute amplitude values.

Electrophysiology in organotypic slice cultures

Cultured slices were prepared and transfected as previously described (Schnell et al., 2002). Briefly, hippocampi were dissected from P7 *Grin1*$^{fl/fl}$ mice and biolistically transfected with pFUGW-CreGFP (Cre was inserted in-frame before EGFP to form a Cre:GFP fusion protein) after 2–3 days in culture. Slices were cultured for an additional 14–20 days before recording. For recording from organotypic slices, ACSF was supplemented with 5 µM 2-chloroadenosine to dampen epileptiform activity, and $GABA_A$ receptors were blocked by a combination of picrotoxin (0.1 mM) and bicuculline (0.01 mM). Synaptic responses and mEPSCs were recorded similarly to acute slices as described above.

Anatomy and Imaging

CA1 pyramidal cells were filled with Alexa Fluor 568 dye through the patch pipette for approximately 10 min. After filling, slices were fixed in 4% PFA/4% sucrose in PBS for 30 min at room temperature, followed by washing at least three times with PBS. Slices were mounted and imaged by using a Zeiss confocal laser scanning microscope. For dendritic analysis, 3D stacks of each neuron were taken by using a 25x oil immersion objective, and the 2D projections were imported into Neurolucida software (MBF Bioscience). The dendritic tree was manually traced and then analyzed by using NeuroExplorer (MBF Bioscience). For spine analysis, 3D stacks of a 100 µm stretch of primary and secondary apical dendrites from 100-200 µm from the soma were collected by using a 63x oil immersion lens, and spines were counted in 3D projection mode using Zeiss software. For statistical analysis Student's t test was used, and data were presented as mean ± SEM.

Supplemental References

Adesnik, H., Li, G., During, M.J., Pleasure, S.J., and Nicoll, R.A. (2008). NMDA receptors inhibit synapse unsilencing during brain development. Proc Natl Acad Sci U S A *105*, 5597-5602.

Akashi, K., Kakizaki, T., Kamiya, H., Fukaya, M., Yamasaki, M., Abe, M., Natsume, R., Watanabe, M., and Sakimura, K. (2009). NMDA receptor GluN2B (GluR epsilon 2/NR2B) subunit is crucial for channel function, postsynaptic macromolecular organization, and actin cytoskeleton at hippocampal CA3 synapses. J Neurosci *29*, 10869-10882.

Bekkers, J.M., and Stevens, C.F. (1990). Presynaptic mechanism for long-term potentiation in the hippocampus. Nature *346*, 724-729.

Bellone, C., and Nicoll, R.A. (2007). Rapid bidirectional switching of synaptic NMDA receptors. Neuron *55*, 779-785.
Clements, J.D., and Westbrook, G.L. (1991). Activation kinetics reveal the number of glutamate and glycine binding sites on the N-methyl-D-aspartate receptor. Neuron *7*, 605-613.

Del Castillo, J., and Katz, B. (1954). Quantal components of the end-plate potential. J Physiol *124*, 560-573.

Goold, C.P., and Nicoll, R.A. (2010). Single-cell optogenetic excitation drives homeostatic synaptic depression. Neuron *68*, 512-528.

Hessler, N.A., Shirke, A.M., and Malinow, R. (1993). The probability of transmitter release at a mammalian central synapse. Nature *366*, 569-572.

Jahr, C.E. (1992). High probability opening of NMDA receptor channels by L-glutamate. Science *255*, 470-472.
Kerchner, G.A., and Nicoll, R.A. (2008). Silent synapses and the emergence of a postsynaptic mechanism for LTP. Nat Rev Neurosci *9*, 813-825.

Li, Y., Erzurumlu, R.S., Chen, C., Jhaveri, S., and Tonegawa, S. (1994). Whisker-related neuronal patterns fail to develop in the trigeminal brainstem nuclei of NMDAR1 knockout mice. Cell *76*, 427-437.

Malinow, R., and Tsien, R.W. (1990). Presynaptic enhancement shown by whole-cell recordings of long-term potentiation in hippocampal slices. Nature *346*, 177-180.

Mishina, M., and Sakimura, K. (2007). Conditional gene targeting on the pure C57BL/6 genetic background. Neurosci Res *58*, 105-112.

Rosenmund, C., Clements, J.D., and Westbrook, G.L. (1993). Nonuniform probability of glutamate release at a hippocampal synapse. Science *262*, 754-757.

Schnell, E., Sizemore, M., Karimzadegan, S., Chen, L., Bredt, D.S., and Nicoll, R.A. (2002). Direct interactions between PSD-95 and stargazin control synaptic AMPA receptor number. Proc Natl Acad Sci U S A *99*, 13902-13907.

Xiang, Z., Greenwood, A.C., Kairiss, E.W., and Brown, T.H. (1994). Quantal mechanism of long-term potentiation in hippocampal mossy-fiber synapses. J Neurophysiol *71*, 2552-2556.